Pure appl. geophys. 158 (2001) 567–603
0033–4533/01/030567–37 $ 1.50 + 0.20/0

© Birkhäuser Verlag, Basel, 2001

Pure and Applied Geophysics

Identification Criteria for Sources of *T* Waves Recorded in French Polynesia

JACQUES TALANDIER[1] and EMILE A. OKAL[2]

Abstract— From a data set of 150 digital records of *T* phases from 71 sources obtained on seismometers of the Polynesian Seismic Network, we define a discriminant separating earthquake and explosion sources, which uses the maximum amplitude of recorded ground velocity, measured on its envelope, e_{Max} (in μm/s), and the duration of the phase measured at 1/3 of maximum amplitude, $\tau_{1/3}$ (in seconds). Earthquake sources and man-made explosions are effectively separated in a log-log space by the straight line

$$\log_{10} e_{Max} = 4.9 \log_{10} \tau_{1/3} - 4.1 \ .$$

Other criteria in both the time and frequency domains fail to reliably separate the populations of the various kinds of events. The application of this technique to analog records of large-scale man-made explosions carried out in the 1960s confirms that it provides an adequate discriminant over 3.5 orders of magnitude of ground velocity.

Key words: Seismic discrimination, hydroacoustics, *T* phases.

1. Introduction and Background

The Comprehensive Nuclear-Test-Ban Treaty (CTBT) has mandated as part of its International Monitoring System (IMS) the deployment of so-called *T*-phase stations, which consist of high-frequency seismometers located in the immediate vicinity of coastlines, for the purpose of recording seismic waves converted from acoustic energy propagated in the SOFAR channel of the world's oceans. The advantage of this design over more traditional hydrophone stations (also mandated by the CTBT) stems from a considerable simplification of logistics for powering, maintenance and data retrieval. It builds on the longstanding observation that the exceptionally efficient propagation of *T* waves in the water mass of the ocean allows the detection and location of very small, very remote sources in the marine

[1] Département Analyse et Surveillance de l'Environnement, Commissariat à l'Energie Atomique Boîte Postale 12, 91680 Bruyères-le-Châtel, France.

[2] Department of Geological Sciences, Northwestern University, Evanston, IL 60201, U.S.A. E-mail: emile@earth.nwu.edu

environment, all from land-based instruments. Indeed, the first positive identifications of T phases were made on seismometers (LINEHAN, 1940; RAVET, 1940).

The routine operation of hydrophone networks over several decades in the Pacific Basin has long established that T phases can vastly increase detection capabilities in the basin (e.g., DUENNEBIER and JOHNSON, 1967), with similar observations at land-based networks, such as the Polynesian Seismic Network (Réseau Sismique Polynésien; hereafter RSP) headquartered in Papeete, Tahiti. Thus, the operational framework for T-phase and hydrophone stations in the IMS is that of the detection and location of an event based entirely on T phases, without the benefit of additional seismic phases, such as P waves. It is also in this context that a further step must be performed, i.e., the identification of the nature of the source as either a natural phenomenon or a man-made explosion.

The purpose of the present paper is to build on a data set of T phases recorded at the RSP over 35 years, both from earthquakes (documented and located from their seismic waves), and from known marine explosions, and to explore systematically a number of criteria in the quest for a reliable discriminant between natural and man-made sources. We show that a comparison between maximum amplitude (determined on a smoothed envelope) and duration at 1/3 of maximum provides a reliable means of separating earthquakes from explosions, which can be applied over 3.5 orders of magnitude of ground velocity signal. We find it imperative, however, to use stations located on atolls which feature a simpler and more efficient acoustic-to-seismic conversion than do volcanic high island sites (TALANDIER and OKAL, 1998).

2. Methodology

Data Set

Table 1 lists the digital data set used in this study, comprising 150 seismograms of T phases from 71 events recorded at short-period seismic stations of the Polynesian Seismic Network (Réseau Sismique Polynésien, hereafter RSP) during the period 1971–1997. This data set is complemented by records from earlier events (1962–1970) of generally much larger amplitudes, and for which the data processing had to be adapted to the analog records available at those dates (Table 2). For this reason, these much larger sources are the subject of a separate discussion in Section 4.

The RSP network, described most recently by TALANDIER (1993), comprises 17 permanent short-period stations. During local refraction campaigns, a number of temporary sites were instrumented. We distinguish in this study between stations located on atolls ("(A)" in Tables 1 and 2) and those on high volcanic islands ("(H)"): we have shown in TALANDIER and OKAL (1998) that the conditions of conversion of seismic energy to and from acoustic (T) energy differ fundamentally for

Table 1

Digital T-wave records used in this study

Date D M (J) Y	Origin Time GMT	Station Code	Site	Nature (†)	CODE NAME (E) or Region (E, S, H, V)	Event size (*)	Reference (§)
9 OCT (282) 1971	18:14	RUV	(A)	E	Polynesia	0.082 t	
9 OCT (282) 1971	18:14	TPT	(A)	E			
30 SEP (273) 1979	12:45	VIV	(A)	V	Macdonald		a
21 AUG (234) 1980	15:00	DIN	(A)	E	Vancouver Is.		
21 AUG (234) 1980	15:00	DOR	(A)	E			
21 AUG (234) 1980	15:00	IRN	(A)	E			
21 AUG (234) 1980	15:00	RUV	(A)	E			
21 AUG (234) 1980	15:00	TPT	(A)	E			
10 NOV (315) 1980	11:26	VIV	(A)	V	Macdonald		a
24 DEC (359) 1980	16:09	AFR	(H)	V			
24 DEC (359) 1980	16:09	VIV	(A)	V			
15 FEB (046) 1981	16:18	VIV	(A)	V			
8 MAR (067) 1981	13:59	VAH	(A)	H	Mehetia	3.1 M_L	b
8 MAR (067) 1981	14:30	VAH	(A)	H	Mehetia	3.3 M_L	b
20 MAR (079) 1981	15:00	VAH	(A)	H	Mehetia	3.1 M_L	b
16 DEC (350) 1981	00:43	VAH	(A)	E	Polynesia	0.082 t	c
11 FEB (042) 1982	18:54	VAH	(A)	E	Polynesia	0.082 t	c
11 FEB (042) 1982	19:15	VAH	(A)	E			
11 FEB (042) 1982	22:04	VAH	(A)	E			
1 MAR (060) 1982	22:37	VIV	(A)	V	Macdonald		d
25 MAR (084) 1982	18:02	VAH	(A)	E	Polynesia	0.082 t	c
25 MAR (084) 1982	18:24	VAH	(A)	E	Polynesia	0.082 t	c
25 MAR (084) 1982	19:58	FGA	(A)	E	Polynesia	0.082 t	c
25 MAR (084) 1982	20:20	FGA	(A)	E	Polynesia	0.082 t	c
14 MAR (073) 1983	19:15	VIV	(A)	V	Macdonald		d
24 MAR (083) 1985	17:05	DOR	(A)	E	PSPM	0.9 t	e
24 MAR (083) 1985	17:05	FGA	(A)	E			
24 MAR (083) 1985	17:05	IRN	(A)	E			
24 MAR (083) 1985	22:04	DOR	(A)	E	PSPM	0.9 t	e
24 MAR (083) 1985	22:04	FGA	(A)	E			
24 MAR (083) 1985	22:04	IRN	(A)	E			
26 MAR (085) 1985	16:03	DOR	(A)	E	PSPM	1.0 t	e
26 MAR (085) 1985	16:03	FGA	(A)	E			
26 MAR (085) 1985	16:03	IRN	(A)	E			
26 MAR (085) 1985	16:03	TPT	(A)	E			
26 MAR (085) 1985	22:05	DOR	(A)	E	PSPM	1.4 t	e
26 MAR (085) 1985	22:05	FGA	(A)	E			
26 MAR (085) 1985	22:05	IRN	(A)	E			
26 MAR (085) 1985	22:05	TPT	(A)	E			
30 MAR (089) 1985	22:01	TPT	(A)	E	PSPM	0.8 t	e
31 MAR (090) 1985	15:33	DOR	(A)	E	PSPM	0.8 t	e
31 MAR (090) 1985	15:33	FGA	(A)	E			
31 MAR (090) 1985	15:33	IRN	(A)	E			
31 MAR (090) 1985	15:33	TPT	(A)	E			
1 APR (091) 1985	18:31	DOR	(A)	E	PSPM	0.5 t	e
1 APR (091) 1985	18:31	FGA	(A)	E			
1 APR (091) 1985	18:31	IRN	(A)	E			

Table 1

(*Continued*)

Date D M (J) Y	Origin Time GMT	Station Code	Site	Nature (†)	CODE NAME (E) or Region (E, S, H, V)	Event size (*)	Reference (§)
1 APR (091) 1985	18:31	TPT	(A)	E			
1 APR (091) 1985	29:31	TPT	(A)	E	PSPM	0.2 t	e
30 MAY (150) 1985	01:22	PMO	(A)	E			
31 MAY (151) 1985	05:42	PMO	(A)	M			
18 AUG (230) 1986	03:37	PMO	(A)	M			
18 AUG (230) 1986	03:38	PMO	(A)	M			
19 AUG (231) 1986	03:59	PMO	(A)	M			
3 SEP (246) 1986	06:04	PMO	(A)	M			
3 SEP (246) 1986	06:05	PMO	(A)	M			
4 SEP (247) 1986	12:38	TPT	(A)	E			
17 SEP (260) 1986	23:29	RUV	(A)	E			
17 SEP (260) 1986	23:29	TPT	(A)	E			
9 DEC (343) 1989	10:00	AFR	(H)	E	MIDPLATE	0.3 t	f
9 DEC (343) 1989	10:00	HUA	(A)	E			
9 DEC (343) 1989	10:00	MEH	(H)	E			
9 DEC (343) 1989	10:00	PAE	(H)	E			
9 DEC (343) 1989	10:00	PPN	(H)	E			
9 DEC (343) 1989	10:00	PPT	(H)	E			
9 DEC (343) 1989	10:00	TIA	(H)	E			
9 DEC (343) 1989	10:00	TVO	(H)	E			
9 DEC (343) 1989	17:00	PPN	(H)	E	MIDPLATE	0.3 t	f
9 DEC (343) 1989	17:00	TIA	(H)	E			
9 DEC (343) 1989	17:00	TVO	(H)	E			
9 DEC (343) 1989	18:00	FGA	(A)	E	MIDPLATE	0.3 t	f
13 DEC (347) 1989	19:45	VAH	(A)	E	MIDPLATE	0.025 t	f
15 DEC (349) 1989	02:00	DIN	(A)	E	MIDPLATE	0.3 t	f
15 DEC (349) 1989	02:00	FGA	(A)	E			
15 DEC (349) 1989	02:00	VAH	(A)	E			
21 DEC (355) 1989	22:42	PMO	(A)	V	Mariana Is.		
21 DEC (355) 1989	23:34	PMO	(A)	V	Mariana Is.		
22 DEC (356) 1989	16:00	MKT	(A)	E	MIDPLATE	1.0 t	f
22 DEC (356) 1989	18:00	MKT	(A)	E	MIDPLATE	0.3 t	f
23 DEC (357) 1989	07:37	PMO	(A)	V	Mariana Is.		
28 DEC (362) 1989	16:00	MEH	(H)	E	MIDPLATE	0.2 t	f
6 MAY (126) 1993	17:39	PMO	(A)	V	Mariana Is.		
8 JUN (159) 1993	12:57	PMO	(A)	H	Hawaii	5.2 m_b	g
8 JUN (159) 1993	12:57	RUV	(A)	H			
8 JUN (159) 1993	12:57	TIA	(H)	H			
8 JUN (159) 1993	12:57	TPT	(A)	H			
27 JUN (178) 1994	18:30	RUV	(A)	E	California		
27 JUN (178) 1994	18:30	TPT	(A)	E			
6 JAN (006) 1995	22:37	PPT	(H)	S	Hokkaido	3.3×10^{26} dyn-cm	h
6 JAN (006) 1995	22:37	TIA	(H)	S			
19 FEB (050) 1995	04:03	PPT	(H)	S	California	9.9×10^{25} dyn-cm	h
19 FEB (050) 1995	04:03	RUV	(A)	S			
19 FEB (050) 1995	04:03	TIA	(H)	S			
19 FEB (050) 1995	04:03	TPT	(A)	S			

Table 1

(*Continued*)

Date D M (J) Y	Origin Time GMT	Station Code	Site	Nature (†)	CODE NAME (E) or Region (E, S, H, V)	Event size (*)	Reference (§)
9 MAR (068) 1995	08:12	TIA	(H)	H	Hawaii	3.9 m_b	g
14 MAR (073) 1995	17:33	AFR	(H)	S	Alaska	2.2×10^{25} dyn-cm	h
14 MAR (073) 1995	17:33	PMO	(A)	S			
14 MAR (073) 1995	17:33	PPT	(H)	S			
14 MAR (073) 1995	17:33	RUV	(A)	S			
14 MAR (073) 1995	17:33	TIA	(H)	S			
14 MAR (073) 1995	17:33	TPT	(A)	S			
1 NOV (305) 1995	00:35	MEH	(H)	S	Chile	1.14×10^{26} dyn-cm	i
1 NOV (305) 1995	00:35	TET	(A)	S			
1 NOV (305) 1995	00:35	TIA	(H)	S			
16 JAN (016) 1996	20:46	TVO	(A)	S			
16 JAN (016) 1996	20:46	VAH	(A)	S			
7 FEB (038) 1996	21:36	PMO	(A)	S	Kuril Is.	6.4×10^{26} dyn-cm	j
7 FEB (038) 1996	21:36	PPT	(H)	S			
7 FEB (038) 1996	21:36	TET	(A)	S			
7 FEB (038) 1996	21:36	TIA	(H)	S			
30 MAR (090) 1996	09:56	AFR	(H)	S	Eltanin F.Z.	1.5×10^{25} dyn-cm	
30 MAR (090) 1996	09:56	VAH	(A)	S			
30 JUN (182) 1996	22:27	AFR	(H)	S	Eltanin F.Z.	1.7×10^{24} dyn-cm	k
30 JUN (182) 1996	22:27	VAH	(A)	S			
22 JUL (204) 1996	10:33	PPT	(H)	H	Hawaii	3.7 M_D	g
22 JUL (204) 1996	10:33	RUV	(A)	H			
22 JUL (204) 1996	10:33	TIA	(H)	H			
22 JUL (204) 1996	10:33	TPT	(A)	H			
23 JUL (205) 1996	03:12	RUV	(A)	H			
23 JUL (205) 1996	03:12	TIA	(H)	H			
23 JUL (205) 1996	03:12	TPT	(A)	H			
23 JUL (205) 1996	05:20	AFR	(H)	S	Kermadec	2.3×10^{25} dyn-cm	l
23 JUL (205) 1996	05:20	PPT	(H)	S			
23 JUL (205) 1996	13:24	PPT	(H)	H	Hawaii	4.6 m_b	g
23 JUL (205) 1996	13:24	RUV	(A)	H			
23 JUL (205) 1996	13:24	TIA	(H)	H			
23 JUL (205) 1996	13:24	TPT	(A)	H			
29 JUL (211) 1996	04:06	PMO	(A)	V	Hawaii	3.9 M_D	g
29 JUL (211) 1996	04:06	RUV	(A)	V			
29 JUL (211) 1996	04:06	TPT	(A)	V			
29 JUL (211) 1996	04:08	RUV	(A)	V	Hawaii		
29 JUL (211) 1996	04:08	TIA	(A)	V			
29 JUL (211) 1996	04:08	TPT	(A)	V			
29 JUL (211) 1996	11:00	PPT	(H)	H	Hawaii	4.4 M_D	g
29 JUL (211) 1996	11:00	RUV	(A)	H			
29 JUL (211) 1996	11:00	TPT	(A)	H			
14 NOV (319) 1996	13:47	PPT	(H)	S	S. of Fiji	1.9×10^{25} dyn-cm	m
16 MAR (075) 1997	14:19	PMO	(A)	H	Hawaii	4.2 M_D	
16 MAR (075) 1997	14:19	PPT	(H)	H			
16 MAR (075) 1997	14:19	TIA	(H)	H			
16 MAR (075) 1997	14:19	TPT	(A)	H			

Table 1

(*Continued*)

Date	Origin Time	Station		Nature	CODE NAME (E) or Region	Event size	Reference
D M (J) Y	GMT	Code	Site	(†)	(E, S, H, V)	(*)	(§)
16 MAR (075) 1997	14:19	TVO	(H)	H			
30 JUN (181) 1997	15:47	PMO	(A)	H	Hawaii	3.7×10^{24} dyn-cm	n
30 JUN (181) 1997	15:47	PPT	(H)	H			
30 JUN (181) 1997	15:47	RKT	(H)	H			
30 JUN (181) 1997	15:47	TBI	(H)	H			
30 JUN (181) 1997	15:47	TIA	(H)	H			
30 JUN (181) 1997	15:47	TPT	(A)	H			
30 JUN (181) 1997	15:47	TVO	(H)	H			
8 JUL (189) 1997	12:11	PPT	(H)	S	Aleutian	6.7×10^{24} dyn-cm	o

(†) E: Underwater explosion; H: Earthquake at hotspot volcanic site; M: Missile fired from submarine; N: High-altitude nuclear test; S: Subduction zone earthquake; V: Explosive volcanoseismic event.

(*) The size of an earthquake (event type S or H) is given when available by its seismic moment M_0 (in units of dyn-cm), otherwise by its PDE body-wave magnitude m_b, or if unavailable by its local magnitude M_L assigned by RSP, or its duration magnitude M_d, assigned by Hawaiian Volcano Observatory. When available, the size of an explosive (E) event is given by its yield expressed in tons of TNT (t).

(§) References to indidual events: a: TALANDIER and OKAL (1982); b: TALANDIER and OKAL (1984a); c: TALANDIER and OKAL (1987b); d: TALANDIER and OKAL (1984b); e: NAVA *et al.* (1988); f: WEIGEL *et al.* (1990); g: PDE (USGS); h: DZIEWONSKI *et al.* (1996); i: DZIEWONSKI *et al.* (1997a); j: DZIEWONSKI *et al.* (1997b); k: DZIEWONSKI *et al.* (1997c); l: DZIEWONSKI *et al.* (1997d); m: DZIEWONSKI *et al.* (1998); n: DZIEWONSKI *et al.* (1999a); o: DZIEWONSKI *et al.* (1999b).

the two types of structure, the low slope of high islands giving rise to a more complex conversion, and hence increasing the duration of the converted signal. In practice, we emphasize in the present study records obtained on atoll stations, where the conversion mechanism is simpler, and hence the records cleaner.

The sources of the T waves can be classified as either natural or man-made. Among natural sources, we distinguish between subduction zone earthquakes, intraplate earthquakes, and explosive underwater volcanic events. Among man-made sources, we identify chemical explosions in the ocean, and presumed firings of missiles from submarines. Among predigital events, we also consider four large atmospheric nuclear tests over Christmas Island in 1962.

Digital Processing

We base our search for satisfactory criteria of identification of the nature of T-wave sources on a systematic processing of the records along the following algorithm.

- RSP digital time series $s(t)$, available at a sampling rate $\delta t = 0.02$ s, are exemplified in the top frames of Figure 1. The length of the time windows analyzed is generally 20.46 s (1024 points) for the smaller signals, or 81.90 s (4096 points) for T waves emanating from larger subduction zone earthquakes. All

Table 2

T-wave records used in study of high-energy sources

Date	Time	Station		Nature	CODE NAME (N) or Region	Event size	Reference
D M (J) Y	GMT	Code (†)	Site	(*)	(E, P, S, H)	(**)	(§)
Analog (paper) records from explosive sources							
15 JUN (166) 1962	16:01	PPT	(H)	N	DOMINIC	0.8 Mt	a
30 JUN (181) 1962	15:21	PPT	(H)	N	DOMINIC	1.3 Mt	a
10 JUL (191) 1962	16:33	PPT	(H)	N	DOMINIC	1.0 Mt	a
11 JUL (192) 1962	15:37	PPT	(H)	N	DOMINIC	3.9 Mt	a
24 MAY (144) 1966	05:49	TAH	(H)	E	California	1 kt	b
06 SEP (250) 1968	02:07	RGI	(A)	E	Aleutian Is.	0.34 kt	b
13 AUG (225) 1969	16:12	RGI	(A)	P	Vancouver Is.	4.6 m_b	b
09 SEP (252) 1969	21:53	RGI	(A)	P	Vancouver Is.		c
01 OCT (274) 1969	17:11	RGI	(A)	P	Vancouver Is.	4.7 m_b	b
28 MAY (148) 1970	17:38	RGI	(A)	P	Vancouver Is.	4.9 m_b	b
04 SEP (247) 1970	21:23	RGI	(A)	P	Vancouver Is.		c
Additional earthquake records (digital)							
29 NOV (333) 1975	14:47	TPT	(A)	H	Kalapana	1.8×10^{27} dyn-cm	d
22 JUN (173) 1977	12:08	PAE	(H)	S	Tonga	1.8×10^{28} dyn-cm	e
15 NOV (319) 1994	23:10	RUV	(A)	S	Vancouver Is.	3.0 M_L	c

(†) TAH: Parameters at PMO extrapolated from unclipped hydrophone record at Papeete; RGI: Parameters estimated for clipped records at PMO from unclipped records across Rangiroa Atoll.

(*) N: Atmospheric nuclear test; E: Confirmed underwater explosion; P: Presumed underwater explosion; H: Earthquake at intraplate hotspot site; S: Subduction zone earthquake.

(**) The size of explosions (N, E) is given by their yield in tons of TNT, as announced by the appropriate agencies. For presumed underwater explosions (P), their size is given, when available, by the body-wave magnitude m_b reported by the USGS. The size of the large earthquakes (event type S or H) is given by their seismic moment M_0 (in units of dyn-cm). Note that the Kalapana event was accompanied by a large submarine slump (MA *et al.*, 1999), so that a moment tensor description may be inappropriate. For the small 1994 event, we give the local magnitude M_L computed by the Pacific Geoscience Centre (Sidney).

(§) References: a: ANONYMOUS (1989); b: *PDE* (USGS); c: This study; d: ANDO (1979); e: LUNDGREN and OKAL (1988).

signals are high-pass filtered ($f \geq 2$ Hz) to emphasize frequencies capable of propagating in the SOFAR channel.

- In order to eliminate rapid fluctuations in the waveshape, the *envelope* $e(t)$ is then obtained by taking the absolute value of the signal, $|s(t)|$, and computing its 1-s (50-point) average in a moving window sliding in increments of 1 sample (0.02 s). The resulting series is then run through a 1-s moving window running average, to eliminate any remaining higher-frequency fluctuations. The purpose of this smoothing is to recover the general shape of the waveform, regardless of rapid fluctuations which may be due to local recording conditions and may not be representative of the true energy in the T wave. Examples of envelopes are shown in the central frames of Figure 1. The width of the sliding window (1 s) was chosen

by trial and error between 0.5 and 2.5 s. The general amplitude of the record is characterized by the maximum value, e_{Max}, of $e(t)$.

- We then compute the *spectrum* of the signal, shown in the bottom frames of Figure 1. Because of limitations inherent in the response of the seismic sensors used at the RSP, we limit all our frequency investigations to $f \leq 16$ Hz.
- Finally, a *spectrogram* is obtained through a classical frequency-time analysis. For shorter signals, windows are 1.26 s (64 points) long, and are lagged 0.64 s (32 points), while for longer signals, the windows and lags are quadrupled. The frequencies studied are between 1 and 16 Hz. Examples of spectrograms are shown on Figure 2.

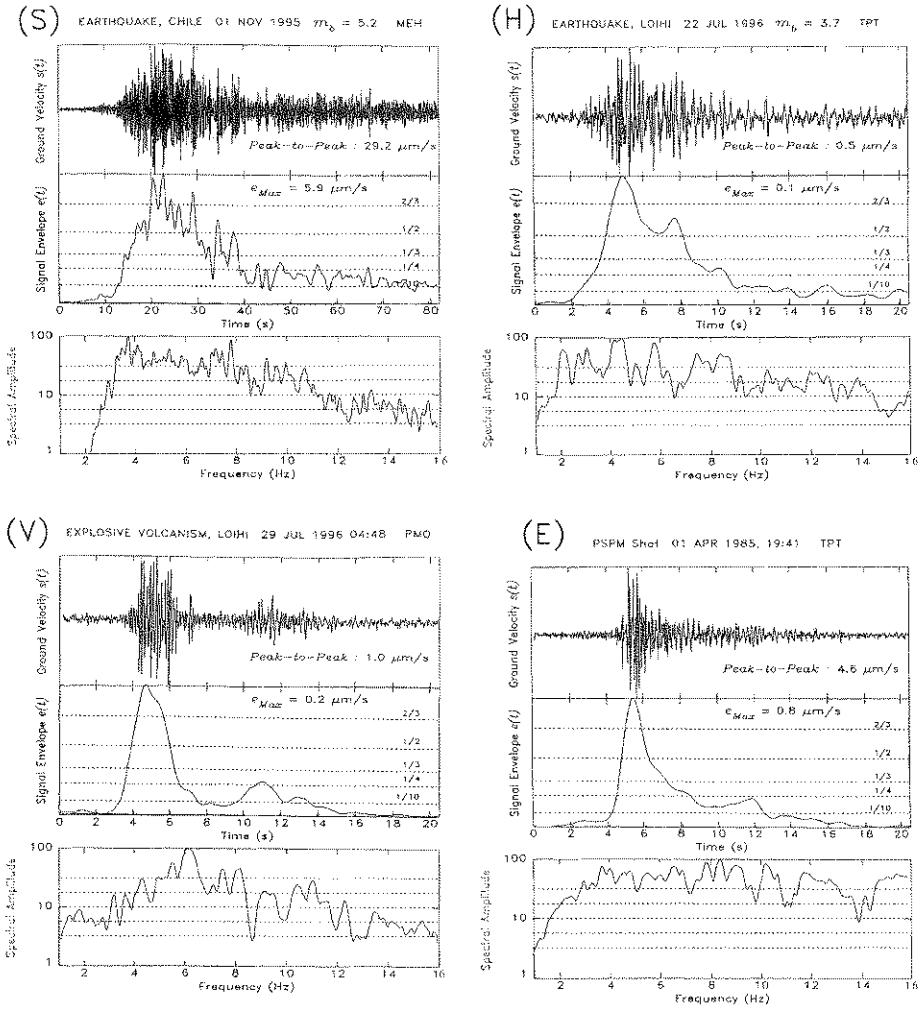

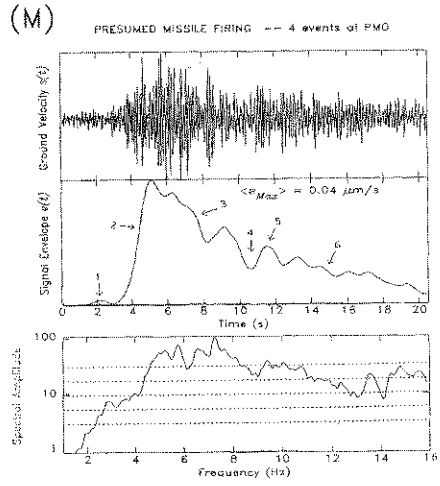

Figure 1

Typical examples of various records of T waves used in this study. **(S):** Subduction zone earthquake; **(H):** Intraplate earthquake; **(V):** Explosive event during a volcanic swarm; **(E):** Man-made underwater explosion; **(M):** Presumed firing of missile from submarine. In each case, the top frame is the deconvolved ground velocity time series $s(t)$ (note the longer window for the subduction event), the middle frame is the envelope $e(t)$, and the bottom frame the spectral amplitude of the signal $s(\omega)$, scaled logarithmically to its maximum value. The horizontal dashed lines in the center frames are the threshold used in the determination of the durations τ_e; similarly those in the bottom frames are the thresholds used in the determination of the width of the spectrum. Because of their low amplitudes, four missile signals have been stacked (with time lags obtained from maximizing their cross correlations) to produce Frame (M).

General Characteristics of Seismograms

Based on typical examples shown on Figures 1 and 2, we describe in this section a number of very general characteristics of the various kinds of sources used.

1. Subduction zone earthquakes (S)

We selected 30 records from 11 earthquakes from the years 1995–1997; a typical T wave is shown on Figure 1(S), and a spectrogram on Figure 2(S).

T-wave records from subduction events usually exhibit a combination of low frequencies, long durations, and emergent waveforms resulting in a spindle-shaped envelope. This can be grossly explained by the following combination of factors: First, the hypocenter of a subduction zone earthquake, typically located at the interface of the colliding plates, will be substantially removed from the water column. The resulting land path before conversion will be long, with high frequencies effectively attenuated before conversion to acoustic energy. The long land path on the source side also favors multipathing, leading to a prolonged waveshape. In addition, subduction events can be large, with sources extending in time for several tens of seconds, and contributing to the duration of the T-wavetrain

(OKAL and TALANDIER, 1986). Finally, the conversion slope will often be shallow-dipping, which requires a complex conversion mechanism involving several reverberations in the water before entrapment by the SOFAR channel can take place, hence the emergent nature of the wavetrain (TALANDIER and OKAL, 1998; PISERCHIA *et al.*, 1998).

We also include in this category T waves from a few transform fault earthquakes in the South Pacific, which were found to exhibit duration characteristics similar to those of subduction events. This can be explained by the absence of steeply dipping converter slopes at the source, even though the hypocenters of the shallower transform earthquakes are located closer to the water mass than those of subduction events.

2. Intraplate earthquakes originating at hotspots (H)

We study 33 records from 10 events with epicenters at the Hawaiian and Society hotspots. A typical example is shown on Figure 1(H) and a spectrogram on Figure 2(H).

In contrast to subduction events, such earthquakes are generally of smaller magnitudes, and very shallow. As such, the shorter seismic paths on the source side allow retention of high frequencies, resulting in a generally whiter spectrum. Also, in geometries such as that of the South Coast of the Big Island of Hawaii, the existence of steep slopes at the head of individual basaltic flows allows a direct and efficient transfer of energy into the SOFAR channel, which results in a generally impulsive wavetrain (TALANDIER and OKAL, 1998).

3. Volcanoseismic explosions (V)

We use 17 records from 8 events, selected from representative periods of activity at Loihi (Hawaii), Macdonald Seamount (Southcentral Pacific), and Ruby (Mariana Islands). A typical signal is shown on Figure 1(V) and a spectrogram on Figure 2(V).

It has long been known that episodes of underwater volcanic activity feature explosive events often interpreted as the release of magmatic conduits opening the way for the eruption of lava into the ocean (TALANDIER and OKAL, 1987a). In particular, such events were observed systematically at the beginning of swarms at Macdonald Seamount (TALANDIER and OKAL, 1982). Since they are presumed to occur at the solid-water interface, they directly generate abundant T waves of relatively short duration, and in the absence of a source-side seismic path, they can feature a high-frequency spectrum. However, certain sources such as Macdonald have spectra limited to $f \leq 10$ Hz.

The explosive nature of these natural sources renders their correct identification and discrimination from man-made explosions a clear challenge. In this respect, it is important to note that volcanoseismic explosions most often

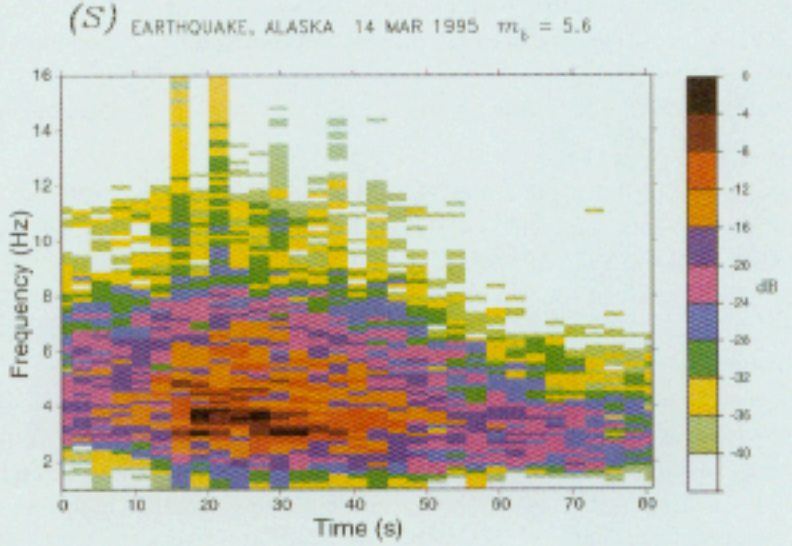

Figure 2(S)
Spectrogram of a typical record from a subduction zone event. The spectral amplitude of ground velocity ($s(\omega, t)$, in units of microns) present in each time–frequency pixel is coded according to the scale bar at right (in dB from maximum spectral amplitude, i.e., $20 \log_{10}[s(\omega, t)/s_{\max}]$). Note the predominance of low frequencies.

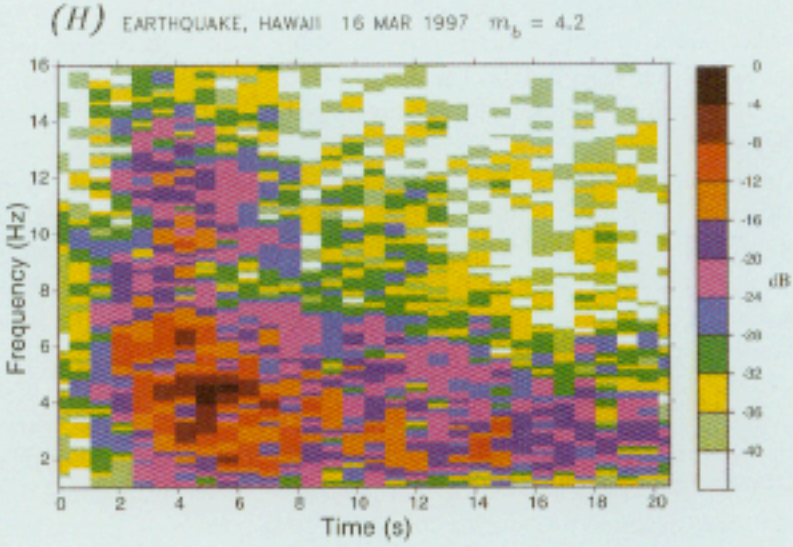

Figure 2(H)
Spectrogram of a typical record from an intraplate earthquake. Note presence of higher frequencies (10–12 Hz) in the early parts of the records.

take place in repetitive, albeit not periodic, sequences. This is clearly shown on Figure 2(V), where a second event is present approximately 12 seconds after the main one.

4. Chemical explosions (**E**)

The main group of explosive sources considered in this study consists of seismic refraction experiments conducted over close to two decades in Polynesia, including the extensive MIDPLATE campaign in 1989 (WEIGEL, 1990); and of the PSPM campaign off the coast of Mexico in 1985 (NAVA *et al.*, 1988). An example of record is shown on Figure 1(E), and a spectrogram shown on Figure 2(E). A total of 64 records from 30 sources were studied.

The generation of sound by explosive sources in the oceanic environment has been the subject of considerable research (e.g., CHAPMAN, 1985). In the framework of this study, such sources can be considered as point sources in time and space. The signals are expected to be of short duration, and to feature high frequencies, but are made more complex by the bubble resonance at a frequency controlled by a combination of source yield and depth (COLE, 1948). However, some firing strategies used in seismic refraction campaigns aim at minimizing the bubble effect (WEIGEL, 1990).

5. Presumed missile firings from submarines (**M**)

During the mid-1980s, a number of *T* waves with very low amplitudes and singular characteristics were recorded principally at Station PMO on Rangiroa Atoll. These were characterized by spectrograms featuring both high frequencies, and a long-source duration (Fig. 2(M)). The former would suggest an impulsive source directly in the water, while the latter requires a phenomenon more complex than a simple explosion.

The occurrence of these signals correlated systematically with the issuance of marine advisories prohibiting navigation over vast expanses of the Northwestern Pacific Basin. On this basis, we speculate that the *T* waves in question were generated during the test-firing of missiles by submerged submarines. A possible scenario, illustrated on the envelope frame of Figure 1(M), would include: (1) a small explosion possibly due to the opening of a valve and the release of the missile; (2) a fast and sharp growth of the signal with white spectrum, corresponding to the underwater firing of the missile; (3) to (4) the slow decay of the signal during the underwater propagation of the missile; (5) a reburst of amplitude when the missile becomes airborne and the rocket is fired; and finally (6) a slow decrease in amplitude during the initial propagation of the rocket in the atmosphere.

Six such records are included in our database.

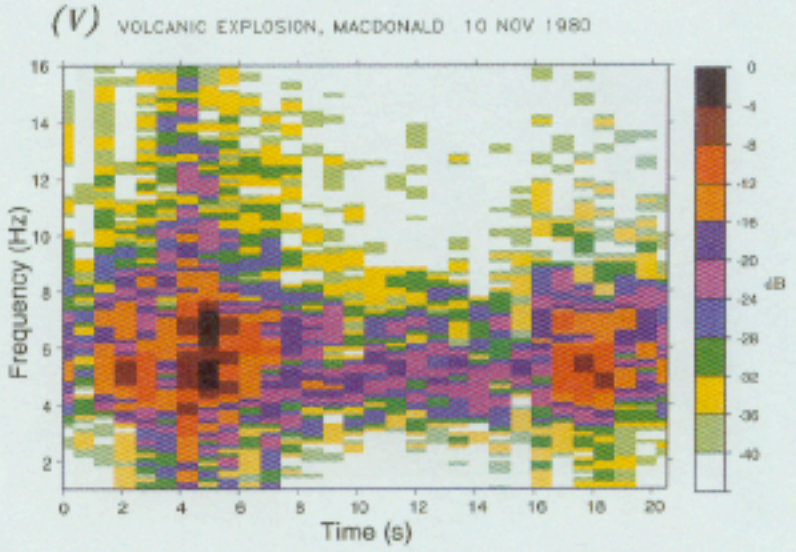

Figure 2(V)
Spectrogram of a typical record from an explosive event during a volcanoseismic swarm at Macdonald Volcano. Note the second event, 17 s into the record, illustrating the repetitive character of this kind of source.

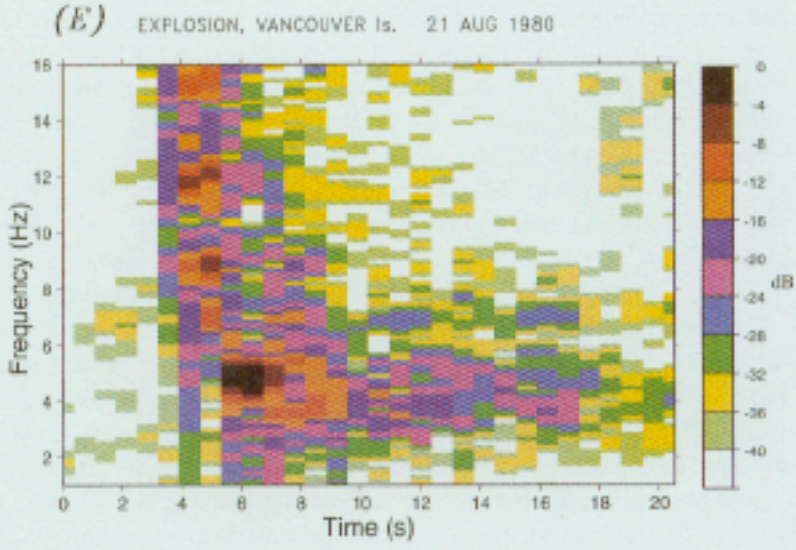

Figure 2(E)
Spectrogram of a typical record from a man-made underwater explosion.

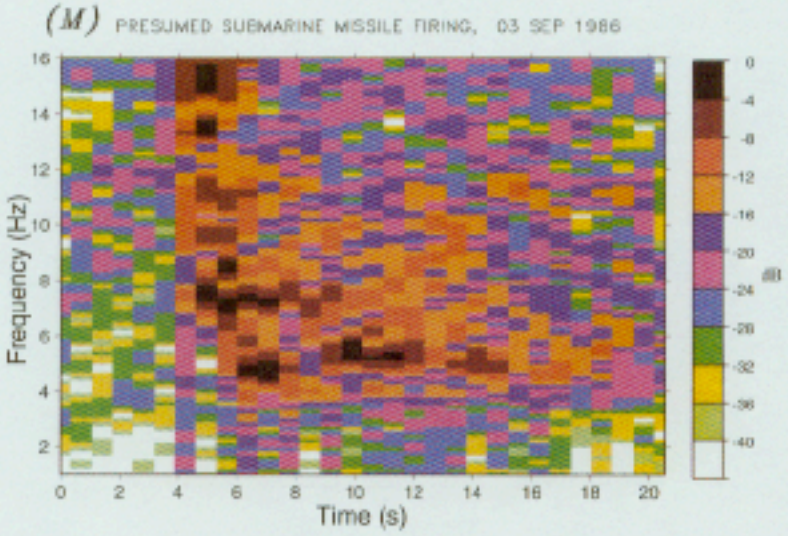

Figure 2(M)
Spectrogram from a presumed underwater missile firing. Note the scattering of the energy over much of the time–frequency plane.

3. Identification of Discrimination Criteria

In this section, we seek robust criteria allowing the discrimination between natural and man-made sources of T waves received at oceanic islands. For this purpose, and on the basis of the processing described above, we define the following parameters, as characteristics of the individual signals. We first focus on the time domain, and compute:

1. The *Maximum Amplitude* e_{Max} of the envelope of the signal. This is of course expected to depend on the epicentral distance traveled by the T wave. We choose here to correct our measurements to a reference distance of 3000 km (or 27° at the surface of the Earth), which can be regarded as typical of transpacific paths. The origin of the decay in amplitude of T waves with distance is, in principle, three-fold: (i) the effect of geometrical spreading at the spherical surface of the Earth; (ii) the effect of intrinsic dispersion during the propagation, and (iii) the possible effect of anelastic attenuation of sound waves in the water. The latter is usually negligible at the frequencies considered here. Because T waves can be considered as mildly dispersed surface waves, the global effect of (i) and (ii) is a decay of amplitude with angular distance Δ, varying like $1/\sqrt{\Delta \sin \Delta}$ (e.g., OKAL, 1989). Thus we will use, in all further discussion and figures, amplitude maxima *corrected* for distance according to:

$$e_{\mathrm{Max}} = e_{\mathrm{Max}}^{\mathrm{Corrected}} = e_{\mathrm{Max}}^{\mathrm{Raw}} \cdot \sqrt{\frac{\Delta}{\Delta_{\mathrm{Ref}}} \frac{\sin \Delta}{\sin \Delta_{\mathrm{Ref}}}} \tag{1}$$

where $\Delta_{\mathrm{Ref}} = 27°$. A number of other empirical distance corrections were tried, notably power laws of the form Δ^{α}, with α ranging from 0.5 to 1.5, with no appreciable influence on our results. This technique obviously requires that the distance to the source be known. In practice, this can be achieved with a regional network, such as the RSP, using at least three stations.

2. The *Duration* τ_r of the signal, defined from the number of points in its envelope reaching a given threshold, $r = 1/10, 1/4, 1/3, 1/2$ or $2/3$, of the maximum amplitude e_{Max}; we will focus primarily on the duration at $1/3$ of maximum, $\tau_{1/3}$.

A difficulty arises from the presence of background noise in the records, the latter varying significantly, not only as a function of time, but even among different stations recording the same event. In order to alleviate this problem, we define the noise level n by considering a 2–second window of record before the arrival of the T phase, and computing the maximum value of its envelope by the same algorithm as in 1. above. The duration τ_r is then defined from the number of points for which the envelope exceeds the level $(n + r\, e_{\mathrm{Max}})$.

3. The *Rise Time* T_R, defined as the time it takes the envelope of the signal to grow from 25% to 100% of its maximum amplitude.

4. Similarly, the *Fall Time*, T_F, defined as the time it takes the envelope of the signal to fall from 100% to 25% of its maximum amplitude.

5. The *Duration of maximum intensity of the signal*, defined as the sum $T_R + T_F$, and representing the time during which the signal keeps a sustained amplitude above $r = 1/4$ of its maximum.

It can differ from the duration $\tau_{1/4}$ as defined in (2), since a complex signal may occasionally fall below the threshold value, and then cross it again. This is especially true for many (but not all) volcanic sources, some intraplate earthquakes, and the largest subduction events.

6. The integrals $I_{\mathrm{env}} = \int e(t)\, dt$ and $J_{\mathrm{inv}} = \int e^2(t)\, dt$ of the envelope over the full window analyzed.

7. The *Skewness Sk* and *Kurtosis Ku* of the signals are defined from their envelope time series $e(t)$ as:

$$Sk = \frac{\int_0^T e(t)(t - \bar{t})^3 dt / \int_0^T e(t)\, dt}{\sigma^3} \tag{2}$$

and

$$Ku = \frac{\int_0^T e(t)(t - \bar{t})^4 dt / \int_0^T e(t)\, dt}{\sigma^4} - 3\ . \tag{3}$$

These quantities are moment estimators which describe the general shape of a statistical variable; in these formulae, $\bar{t}$ and σ are the centroid time of the envelope, and the standard deviation of t, respectively:

$$\bar{t} = \frac{\int_0^T e(t) t \, dt}{\int_0^T e(t) \, dt}; \qquad \sigma^2 = \frac{\int_0^T e(t)(t-\bar{t})^2 \, dt}{\int_0^T e(t) \, dt} \quad . \tag{4}$$

Because they feature a slower buildup of strain release, as well as a longer source duration, earthquake sources would, in principle, be expected to generate signals with lower values of both *Sk* and *Ku*, as compared to higher values of these coefficients for explosion signals.

8. In addition, we also investigate the correlation between the shape of a signal's envelope, and that of reference signals, as detailed in Section 3.

9. In the frequency domain, we define:

The *mean frequency*, $\langle f \rangle$, as the average of those frequencies maximizing the spectral amplitude in each sliding time window of the spectrograms;

10. The *maximum frequency*, f_{Max}, as the greatest among those frequencies maximizing the spectral amplitude in each sliding time window of the spectrograms;

11. The *width of the frequency spectrum*, measured as the number of points, in the spectral domain, for which the spectral amplitude $X(\omega)$ is greater than a given fraction a of its maximum value. This parameter is computed for the values $a = 1/3.2$, $1/5.6$, $1/10$, $1/32$ and $1/56$, which constitute a geometrical progression of ratio $r = 10^{-1/4}$.

12. Finally, we consider the *ratio of low- and high-frequency energy* (R_{LH}), defined as the ratio of the integral of the energy in the two bandwidths $2 \leq f \leq 9$ Hz and $9 \leq f \leq 16$ Hz.

The Failure of Simple Criteria in the Frequency Domain

The idea of seeking a discriminant in the frequency characteristics of the signals stems from at least two properties: first, explosions are expected to be shorter-lived than earthquakes, thus generating high-frequency spectra; and second, earthquake sources being removed from the conversion point, will see their higher frequencies attenuated over the source-to-conversion path. One would then expect explosions to be separable from earthquakes, on the basis of a higher-frequency spectrum.

However, the examination of the spectra on Figures 1(H) and 1(E) shows that both are remarkably "white." Similarly, the spectrograms on Figures 2(H) and 2(E) show that both kinds of signals can feature high frequencies (in the range of 10–12 Hz) in the earliest parts of the signal. In order to analyze this situation further, we carried out the following investigations:

1. Mean frequency

On Figure 3a, we plot the maximum envelope amplitude e_{Max} against $\langle f \rangle$. While the lowest mean frequencies ($\langle f \rangle \leq 4$ Hz) are exclusively found in records of earthquakes (subduction or intraplate), and the highest ones ($\langle f \rangle \geq 7.5$ Hz) for explosions (man-made or volcanic), the intermediate field of $\langle f \rangle$ values is populated with all types of records. No trend with amplitude is present, and no separation can be achieved, especially between man-made explosions and intraplate earthquakes.

2. Maximum frequency

As shown on Figure 3b, the results are fundamentally similar (except of course for a change of frequency scale) when using f_{Max} instead of $\langle f \rangle$.

3. Width of spectrum

Figure 4 plots e_{Max} against the width of the spectrum, measured at 1/5.6 of its maximum value. Once again, it is clear that no separation between the various kinds of sources can be achieved on the basis of these parameters. While it is generally true that subduction earthquakes have narrower spectra than other sources, intraplate earthquakes, especially those of smaller magnitude, can feature spectral widths as high as 13 Hz. Also, and rather surprisingly, we find that the spectral width of explosion signals vary over the whole range from 4 to 14 Hz. The elimination (in Fig. 4b) of stations on high islands does not improve the picture. Finally, a variation in the threshold used for the amplitude of the spectrum (from 1/3.2 to 1/56 of its maximum value) does not help either.

4. High-to-low frequency spectral ratio

Figure 5 explores the behavior of the ratio R_{LH} between the energy present in the signal in the low- and high-frequency bands. It is found to be largest ($R_{LH} > 10$) only for subduction earthquakes and certain volcanic explosions, and smallest ($R_{LH} < 2$) for man-made explosions and certain other volcanic events. However, the majority of the data points fall within the range $2 < R_{LH} < 10$ where the different types of sources cannot be separated. No correlation with source size (as expressed by e_{Max}) can be recognized. These results are not changed when stations from high islands are removed (Fig. 5b).

As a conclusion of these four tests in the frequency domain, we confirm that trends do exist along expected properties: subduction earthquakes have signals with generally lower frequencies and narrower spectra than do explosions. However, these trends are far from universal, and the large number of exceptions that they suffer prevents the use of any of the four studied criteria as a reliable discriminant between the various sources. In particular, intraplate earthquakes and explosions can have very similar frequency characteristics.

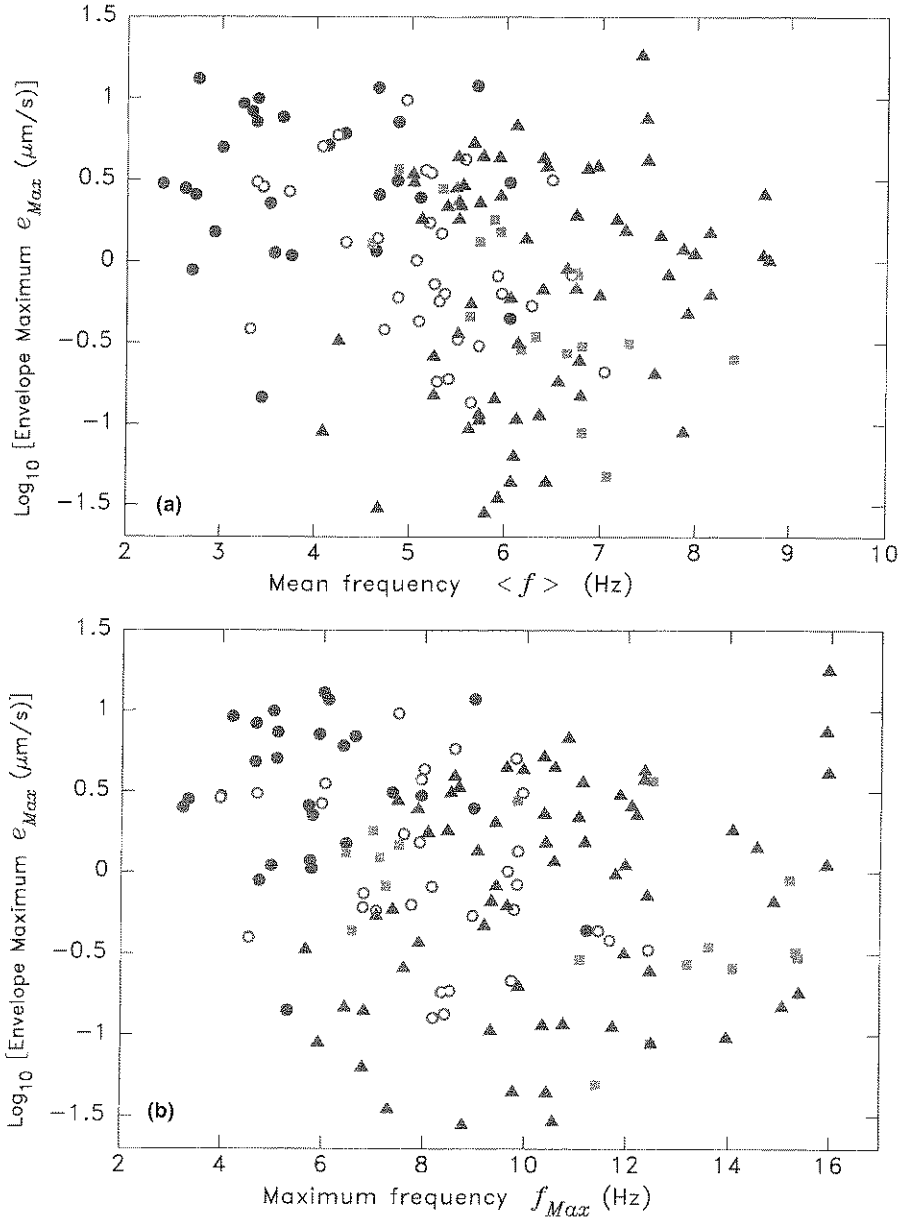

Figure 3

(a) Maximum of signal envelope, e_{Max}, plotted against the mean frequency $\langle f \rangle$. The following symbols are used to differentiate the various sources: *Solid circles*: Subduction earthquakes; *Open Circles*: Midplate earthquakes; *Solid squares*: Explosive volcanic events; *Triangles*: Man-made explosions. Records from both atoll and high island sites are used. Note that this property cannot be used to separate the various populations of events. (b): Same as (a) for the maximum frequency f_{Max}.

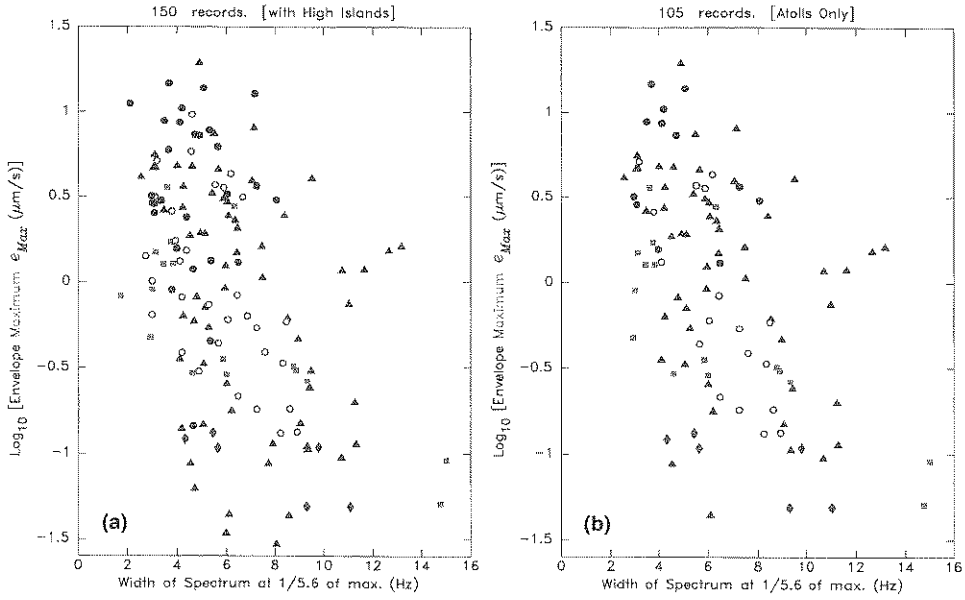

Figure 4
Maximum of signal envelope, e_{Max}, plotted against the width of the Fourier spectrum of the signal, measured at a fraction $a = 1/5.6$ of its maximum. (a): Entired data set; (b): Atoll stations only. Symbols as on Figure 3, complemented by *Diamonds*: Presumed firing of missiles. Note the absence of a clear separator.

Identification of Criteria in the Time Domain

We now turn our attention to potential discriminants related to time-domain characteristics of the signals.

1. Duration as a function of amplitude: The preferred discriminant

We compare here the maximum amplitude of the envelope of the T phase, e_{Max}, with its duration $\tau_{1/3}$ at 1/3 of maximum (Fig. 6). It is clear from this figure that the comparison of these two parameters allows a general separation of earthquakes from explosions, with the former exhibiting a longer duration for a similar level of amplitude. We define empirically the line

$$\log_{10} e_{\mathrm{Max}} = 4.9 \log_{10} \tau_{1/3} - 4.1 \tag{5}$$

where e_{Max} is in μm/s and $\tau_{1/3}$ in s, as an adequate separator in the $\tau_{1/3} - e_{\mathrm{Max}}$ plane. We note that all subduction earthquakes fall clearly to the right of the line, as do all, except two, midplate earthquakes. These two exceptions are shown as bull's eye symbols on Figure 6. The first one, marginally misidentified by the separator, is a small earthquake at Mehetia ($M_L = 3.3$) recorded at VAH on the Southern Coast of Rangiroa Atoll. The second one concerns an earthquake in

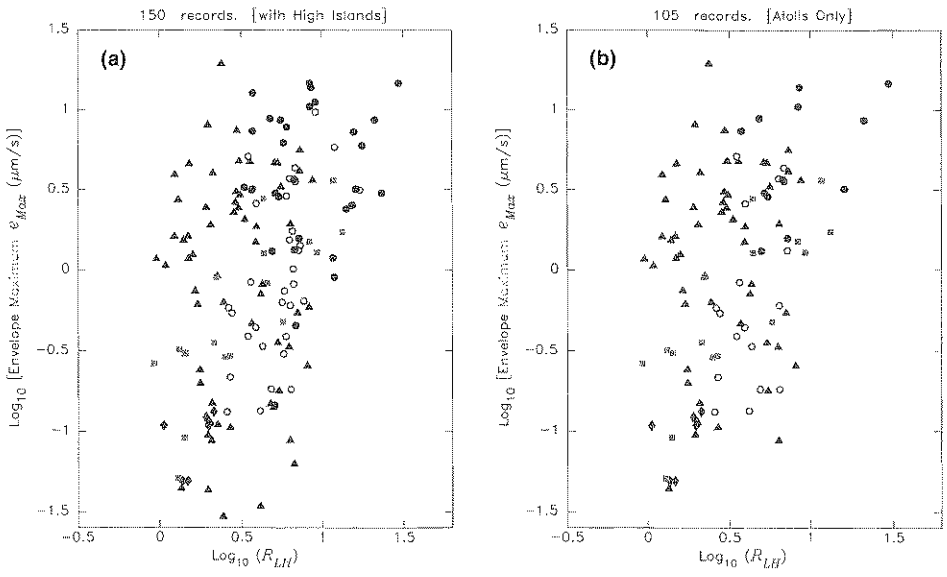

Figure 5
Maximum of signal envelope, e_{Max}, plotted against the ratio R_{LH} of the energies present at low and high frequencies. Symbols as in Figure 4. (a): Full data set; (b): Atoll sites only.

Hawaii ($m_b = 4.2$) recorded at TPT, on the Northern Coast of Rangiroa. It is worth noticing that the same event is correctly identified on its record at PMO. On the other hand, all man-made explosions fall to the left of the line. Volcanic explosive events cannot be discriminated. Finally, presumed firings of missiles (M) are distinguished from explosions, due to the length and complexity of the source process.

In a series of other trials, we investigated the sensitivity of the discriminant to the factor r (taken above as 1/3) defining the duration τ_r. Similar attempts were performed with $r = 1/10$, 1/4, 1/2 and 2/3, and the value $\tau = 1/3$ was found to provide the best results, between values of r too close to 1, for which the concept of duration loses its meaning, and small values which increase the window studied and allow possible contamination by low-energy scatterers.

Finally, on Figure 7, we explore the possibility of including records obtained at high island sites ("(H)" in Table 1). For the bigger events, with the larger envelope amplitudes, the data sets of explosions and earthquakes remain distinct, and a separator can be found (indeed the discriminant (5) remains effective). At the lower amplitudes, post-conversion scattering and multi-pathing on the receiver side can contribute substantially to the duration of the signal, even in the case of an explosion, and the separation becomes impossible. We verified that a similar pattern of degradation of the discriminant at high-island sites occurs for the other threshold levels r defining τ_r.

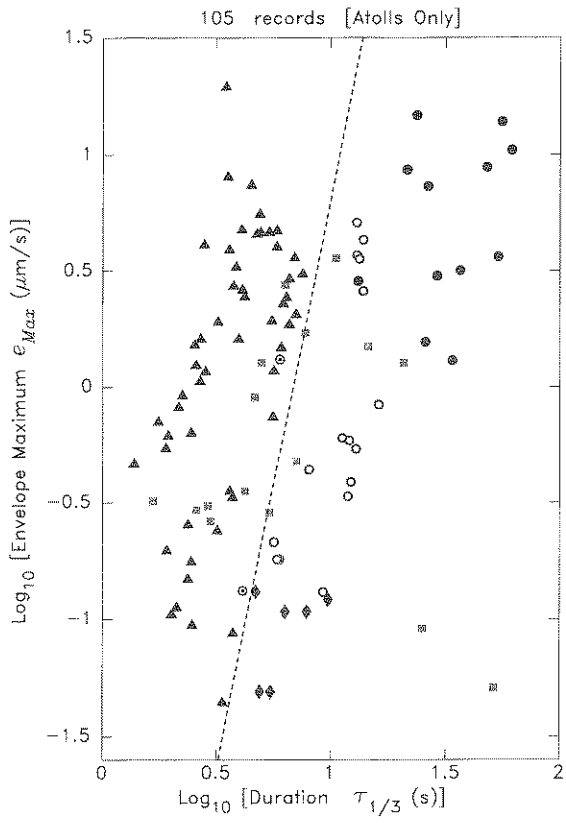

Figure 6

The duration-amplitude discriminant. This figure plots the envelope maximum e_{Max} as a function of signal duration measured at 1/3 of maximum, $\tau_{1/3}$. Symbols as in Figure 4, with the two bull's eye symbols showing the misidentified midplate earthquakes (see text for details). The dashed line is the separator proposed in Equation (5). This figure includes only records obtained at atoll stations.

The comparison between Figures 6 and 7 illustrates the importance of siting *T*–phase stations at shorelines with favorable conversion characteristics, i.e., on atolls or on volcanic structures featuring a steep slope (TALANDIER and OKAL, 1998).

2. Examination of other potential discriminants: Rise Time

Figure 8a explores the potential use of the rise time T_R as a discriminant. This is a legitimate suggestion, since the impulsive nature of an explosive source should lead to rise times shorter than for earthquakes. While subduction zone earthquakes are efficiently separated from explosions, a number of intraplate "hotspot" events are not. In seeking a possible explanation to this pattern, we note that the rise time of a *T*-wave signal is controlled by a combination of the rise time of the source (which can

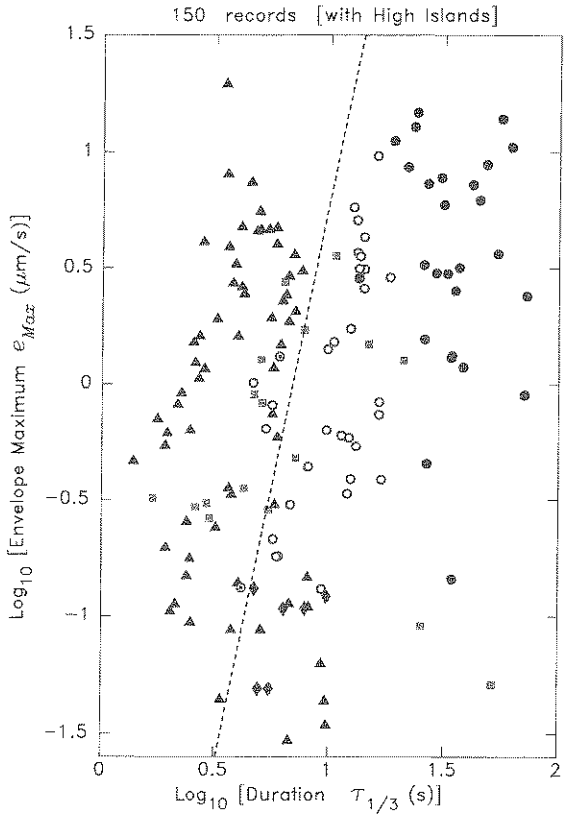

Figure 7
Same as Figure 6, but including records obtained at high island sites. Note the deterioration of the discriminant's performance.

be very short for small earthquakes), and of the buildup of the T phase at the conversion point. We have shown (TALANDIER and OKAL, 1998) that in favorable environments such as the southern shore of the Big Island, the T wave can be generated with a very impulsive wave shape. In addition, and especially for small events, the measure of rise time involves sub-second characteristics of the waveshape, which can then be affected by the slight dispersion observed over the longer paths. This effect is particularly visible at Rangiroa in the case of the 1985 PSPM shots.

In conclusion, we reject rise time as a satisfactory discriminant.

3. Fall time

We similarly investigate on Figure 8b the behavior of the fall time T_F. The situation is, if anything worse, in that even several subduction earthquakes now fail to be separated from the cluster of explosion records. We similarly discard fall time as a satisfactory discriminant.

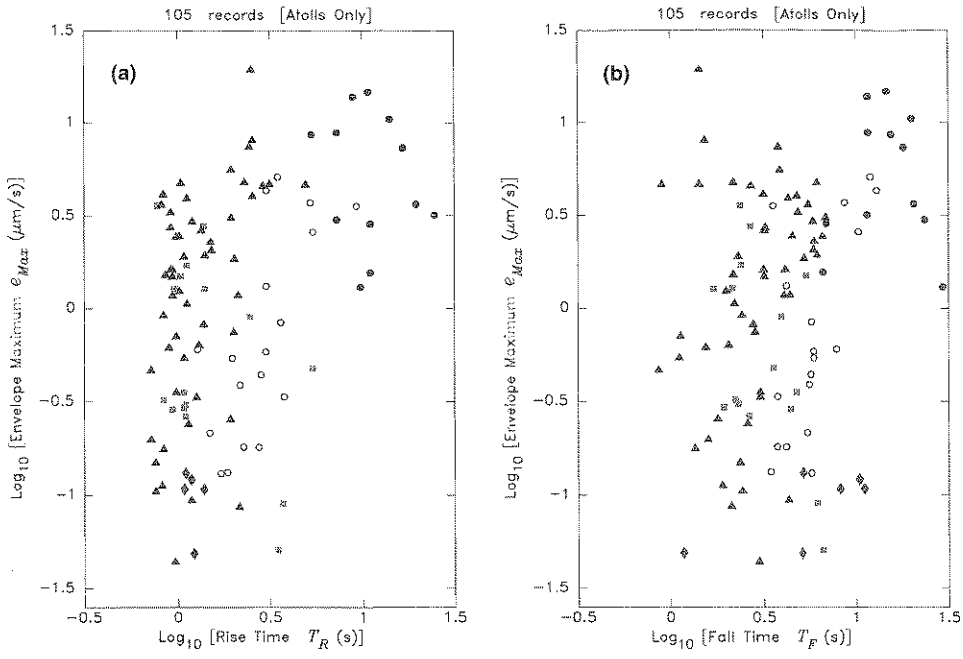

Figure 8
(a): Maximum envelope amplitude as a function of rise time T_R (symbols as in Fig. 4). Note that while subduction earthquakes are adequately separated from explosions by this criterion, intraplate events are not. (b): Same as (a) for the fall time, T_F. Note the failure of this parameter as an adequate discriminant.

4. Total duration T_{Total}

This parameter is the sum of the rise and fall times, and approaches the duration $\tau_{1/4}$ at the threshold used to define T_R and T_F. As expected, when plotted against the maximum amplitude derived from the envelope (Fig. 9a), this parameter does provide a reasonable discriminant. However, its performance is inferior to that of the duration $\tau_{1/4}$, and *a fortiori*, $\tau_{1/3}$, in particular for most intraplate earthquakes, and for the smaller explosions.

Another potentially interesting comparison is that of T_{Total} with the duration $\tau_{1/4}$ itself (Fig. 9b), which illustrates the smoothness of the envelope series $e(t)$. An explosion could be expected to have a simple source time history, and thus a smooth envelope and a T_{Total} identical to $\tau_{1/4}$; on the other hand, an earthquake's more complex source could lead to several crossings of the envelope threshold $r = 1/4$, and thus to a a longer $\tau_{1/4}$, i.e., to a point plotting substantially below the dashed bisector on Figure 9b. Unfortunately, while this trend is indeed present, it is not universal: we find both earthquake records with smooth envelopes, even among the larger subduction events, and explosion records where T_{Total} is deficient by as much as a factor 2.5. In this respect, a discriminant based on this comparison would be far from foolproof, and cannot be proposed.

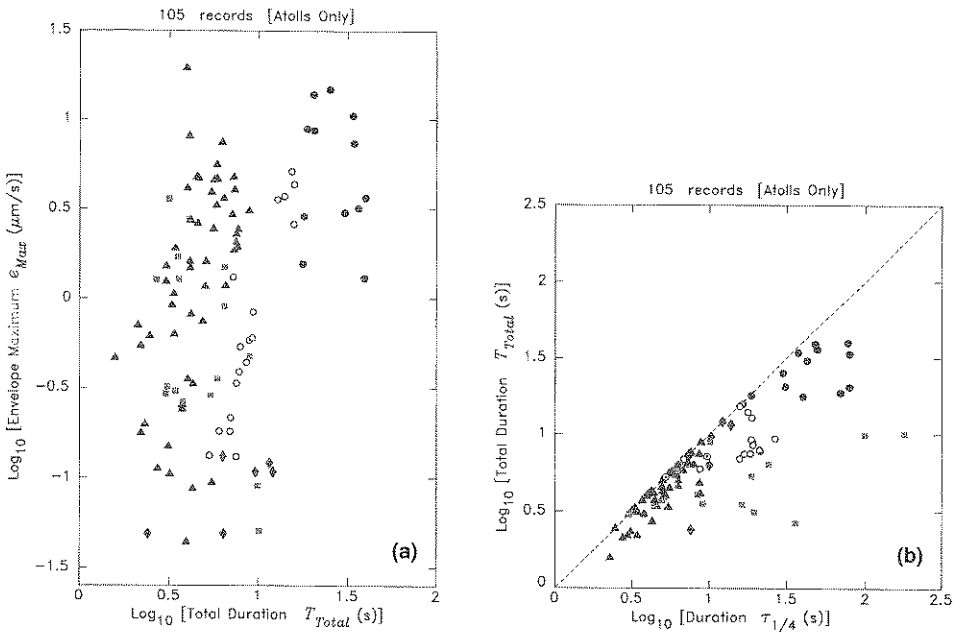

Figure 9
(a): Maximum envelope amplitude as a function of the total duration T_{Total} of sustained amplitude. Note the degradation of the separation in the case of smaller explosions. (b): Comparison of T_{Total} and $\tau_{1/4}$.

5. Skewness and Kurtosis

Pursuing a similar philosophy, we explore on Figure 10 the performance of the parameters *Sk* and *Ku* defined in Equations (2) and (3). The parameters are conveniently plotted against e_{Max} on frames (a) and (b), and against each other on frame (c). We find, once again, that the trend towards lower values of *Sk* and *Ku* for earthquake sources is correctly upheld by the end members of the distribution, but that the intermediate field ($Sk \sim 1$; $Ku \sim 0$) is populated by both earthquakes (mostly intraplate) and explosions. No trend with amplitude can be detected, and the inclusion of records at high island sites (d) worsens the situation. We thus discard skewness and kurtosis as effective discriminants.

6. Envelope integral

Figure 11 correlates the maximum envelope amplitude, e_{Max}, with the integral of the envelope, I_{env}, over the full time window retained for study. While the dashed line

$$\log_{10} e_{\text{Max}} = 9.20 \log_{10} I_{\text{env}} - 22.90 \tag{6}$$

does provide a separation between earthquakes and explosions, the latter is less frank and hence less adequate than the $[e_{\text{Max}} : \tau_{1/3}]$ criterion described above in Equation

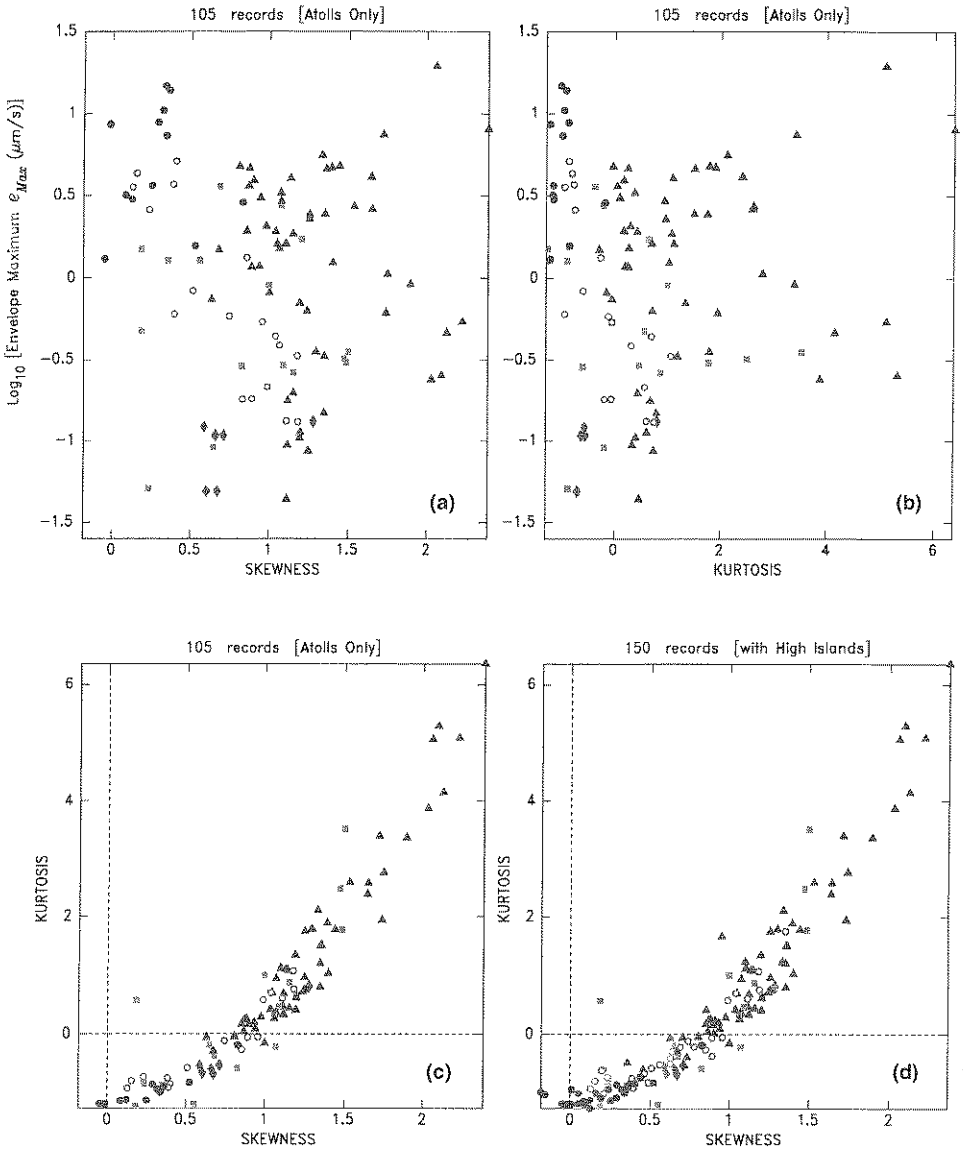

Figure 10

Performance of Skewness (a) and Kurtosis (b) estimators, as defined by Equations (2) and (3), and plotted as a function of e_{Max}, for 105 records at atoll sites. Frame (c) plots *Ku vs. Sk*, and (d) shows further deterioration of their performance when high-island sites are included.

(5). In particular, data points from the intraplate earthquakes are now regrouped very close to the separation, with three (as opposed to two on Figure 6a) straddling it. The use of the energy integral J_{env} instead of I_{env} would, if anything, degrade the results.

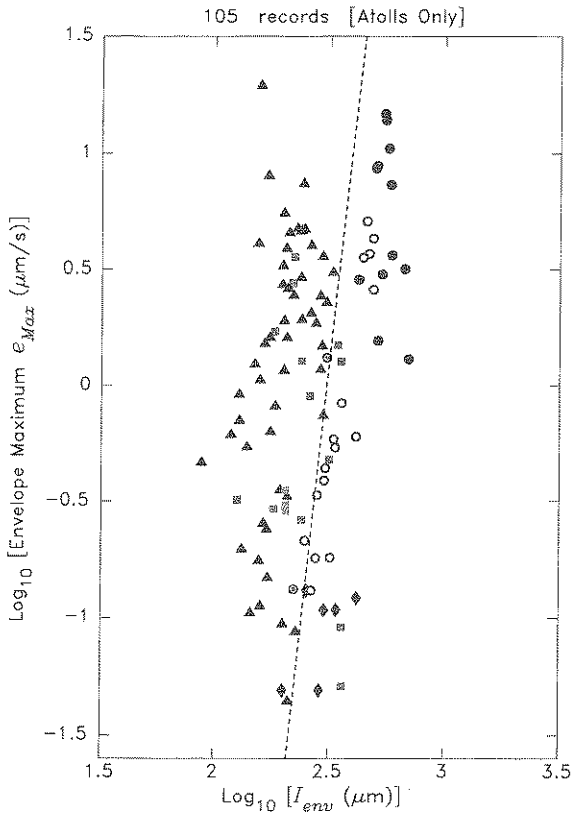

Figure 11
Maximum envelope amplitude as a function of the envelope integral I_{env}. Note that although the dashed line (Equation (6)) can be proposed as a discriminant, the separation is poorer than on Figure 6.

7. Reference envelopes

We define on Figure 12 *reference envelopes*, obtained by stacking, within each family of records (S, H, V, E), the envelopes of the relevant signals, after time-lagging them to align their maxima. The data set has been separated into nearby and distant events in order to examine the case of intraplate earthquakes (H) recorded at short distances. We confirm from this figure that the average waveshape of man-made explosion signals is similar to that of volcanic explosive signals, and to that of intraplate earthquakes, when the latter are recorded at short distance. On the other hand, distant earthquakes (of both types) have a characteristically broader envelope.

We further investigated these properties by computing for each record an envelope misfit, m, defined by taking the integral of the absolute value of the

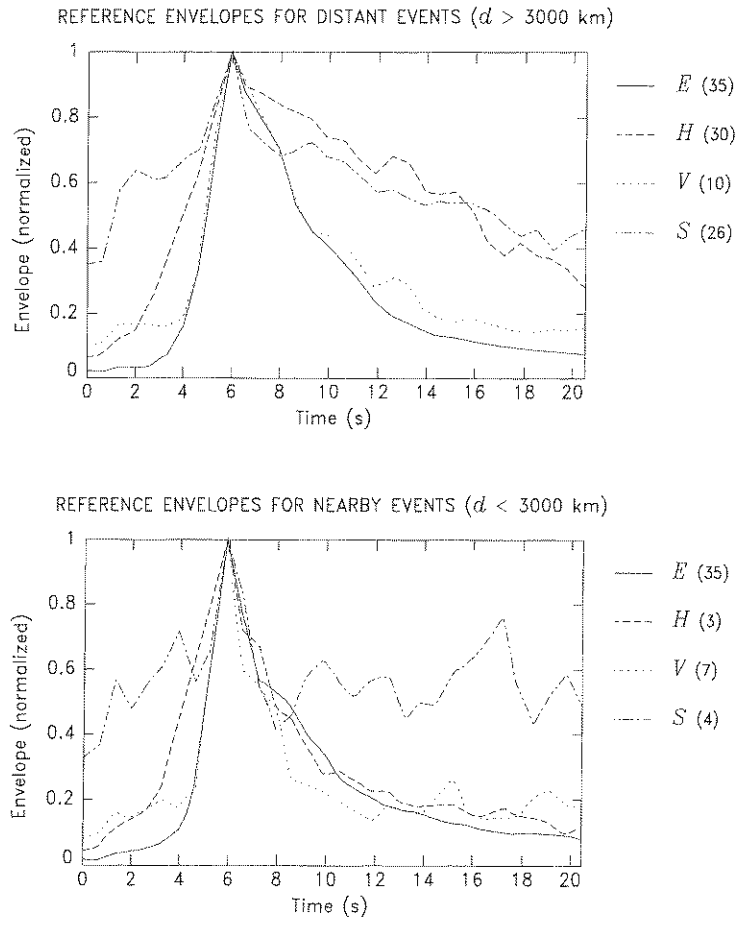

Figure 12
Reference envelopes computed by stacking the envelope signals $e(t)$ within each family of records. Given at right is the number of records stacked to obtain each trace.

misfit between the signal's normalized envelope, and the reference envelope for a particular class of signals, lagged by the time t' for which the maxima coincide,

$$m = \int \left| \frac{e(t)}{e_{\text{Max}}} - e_{\text{Ref}}(t - t') \right| \cdot dt \ , \tag{7}$$

the domain of integration being that over which the envelope is at least 10% of its maximum value, in order to avoid the contribution of background noise. Figure 13, drawn in the case of reference to a subduction event envelope (all distances included), shows that many records are indeed identified properly: subduction records have in

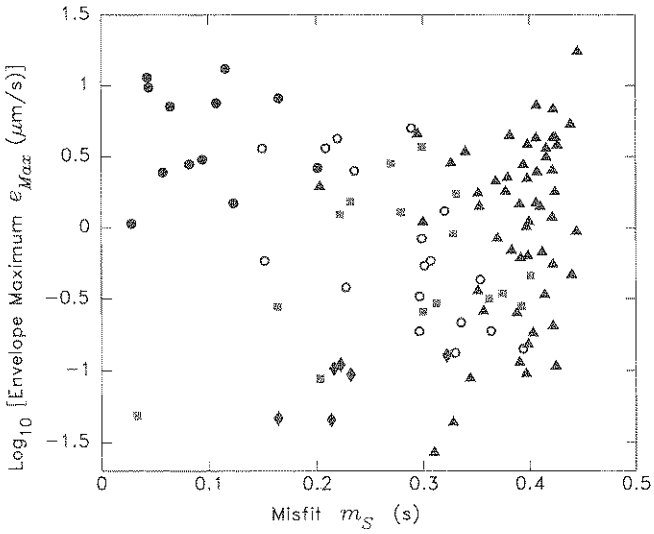

Figure 13
Misfit m_S computed relative to the subduction reference envelope.

general the lowest values of misfit m_S, and the largest ones are found for explosions. However, no reliable criterion for discrimination can be built, since the distinction between the various populations is not sharp, especially between explosions and hotspot earthquakes. We reached a similar conclusion with misfits m_E computed using the explosion envelope as reference.

4. Discussion

From the large number of tests described above, it appears that the comparison of the amplitude of the envelope of the signal, e_{Max}, and its duration at 1/3 of maximum, $\tau_{1/3}$, can be used as an efficient discriminant between tectonic earthquakes and underwater explosions. Another possible discriminant based on the envelope of the signal would use its maximum amplitude e_{Max} and its integral I_{env}. The former discriminant is preferred on account of its better resolution. However, in addition to the two small intraplate earthquakes mentioned above, the discriminant fails in a number of cases which deserve comment.

- Records from explosive events occurring during volcanoseismic swarms are not discriminated. Their characteristics can make them look either like earthquakes or explosions. Indeed, on all diagrams from Figures 3 to 13, the "V" records (plotted as squares) are found in the same fields as explosions (triangles) or earthquakes (especially intraplate; circles). To a large extent, this is due to the

explosive nature of the phenomenon itself, which makes it futile to attempt to distinguish such sources from man-made explosions. However, one property can be used to discriminate easily between "V" and "E" sources: Volcanoseismic swarms are always long-lived on the scale of the duration of individual *T*-wave signals, with explosive events always repetitive, and their occurrence *not* periodic, but rather random in time. The amplitude of the signal also varies with each individual source. In addition, the individual events are separated by intervals of time featuring sustained *T*-wave activity at lower amplitudes, which TALANDIER and OKAL (1987a) have described as expressing the actual delivery of lava onto the ocean floor, following the opening of conduits during the explosive events. These properties are in contrast with our observations during occasional campaigns featuring multiple man-made explosions. As shown for example on Figure 1 of OKAL and TALANDIER (1986), the latter are characterized by perfect periodicity, both in time and amplitude. Also, no detectable activity is present between the various sources, when the *T*-wave signal falls back to the amplitude of background noise. This property makes it easy to discriminate volcanic explosions from man-made ones.

• A second type of signals which does not lend itself well to discrimination is the set of presumed missile firings, although they are generally categorized as "earthquakes" under the discriminant (5), because of the complex nature of their source. Still, they can be recognized through their combination of very small amplitudes, long durations, and abundance of high frequencies. One data point (for the record of 19 August 1986) falls almost exactly on the separator on Figure 6. It features a significantly shorter signal than the other presumed missile firings, in particular those on the previous day; it also features greater values of the coefficients *Sk* and *Ku*. We speculate that it could represent an unsuccessful test, when the missile went astray and failed to become airborne.

Application to Larger Sources

In the framework of the CTBT, it is also important to evaluate the performance of a discriminant such as $[e_{\mathrm{Max}} : \tau_{1/3}]$ in the case of more energetic sources. Unfortunately, no man-made underwater explosions of truly large amplitude were recorded by RSP since the implementation of digital recording in the early 1970s. For this reason, we carry out in this section a more tentative analysis of analog (paper) records obtained in Polynesia from a number of very large explosions carried out in the 1960s and early 1970s and listed in Table 2. These include two major, announced, shots off California in 1966 (1 kt) and the Aleutians in 1968 (0.3 kt), and five events off the coast of Vancouver Island in 1969–1970. Among the latter, three were located by the USGS and ISC, within a few km of 48.47°N, 126.55°W, and given magnitudes m_b between 4.6 and 4.9. We located the other two at a similar epicenter from their *T*-phase records at the RSP. The nature of all five

sources is unpublished, but based on the characteristics of their T waves, we propose that they are indeed explosions.

We also include in the data set digital records from three additional earthquakes. Two of them are events having generated exceptionally intense T waves, the 1977 Tonga event whose T waves woke up residents on the western shore of Tahiti (TALANDIER and OKAL, 1979) and the 1975 Kalapana earthquake, the largest recorded from a Pacific hotspot. The final event is a small ($M_L = 3.0$) 1994 earthquake located in the immediate vicinity of the Vancouver events.

Finally, we study paper records of T waves obtained at Papeete from four atmospheric nuclear tests carried out at Christmas Island in June-July 1962 as part of operation DOMINIC (ANONYMOUS, 1989).

Because no digital records are available for these large underwater events, no data processing can be performed in the frequency domain. In the time domain, the situation is aggravated by the fact that several records are significantly clipped. The 1966 Californian shot predates the instrumentation of Rangiroa Atoll, but we were able to extrapolate the amplitude of the unclipped record on a pressure sensor located in the Tahiti lagoon, to estimate an amplitude of 200 μm/s at station PMO (or 400 μm/s once corrected for distance). In the case of the more recent Aleutian and Vancouver shots, we similarly extrapolate the clipped amplitudes at TPT from unclipped records at other, less favorably located stations on Rangiroa Atoll, based on comparison with digital records of lower amplitudes obtained at later dates from similar locations. The resulting amplitudes must be considered tentative, and we assign them an error of a multiplicative or divisive factor of 2 (± 0.3 logarithmic units). On the other hand, the duration of the signal can be measured from the unclipped records, with a precision of ~25%, or ± 0.1 logarithmic unit. We show the resulting seven data points (with error ellipses) as the large triangles on Figure 14 (we use downward-pointing triangles for the five Vancouver events since their nature as explosions is unconfirmed).

It is remarkable that these seven data points and the two large Tonga and Kalapana earthquakes are perfectly separated by the $[e_{\mathrm{Max}} : \tau_{1/3}]$ discriminant, which was derived for records with amplitudes at least one order of magnitude smaller. Based on the reported explosive nature of the California and Aleutian events, we conclude that the discriminant can be extended to the relevant domain of amplitudes, and we propose that the five Vancouver events are indeed man-made explosions. This interpretation is upheld by the qualitative observation of very high frequencies (estimated at 10 Hz) in the initial phases of the clipped records at TPT. In addition, the small 1994 earthquake selected for study with an epicenter only 40 km from those of the 1969–1970 events clearly has properties characteristic of a plate boundary ("S") event, and fundamentally different from those of the five 1969–1970 events. This effectively rules out the possibility that the latter could be seismic in origin.

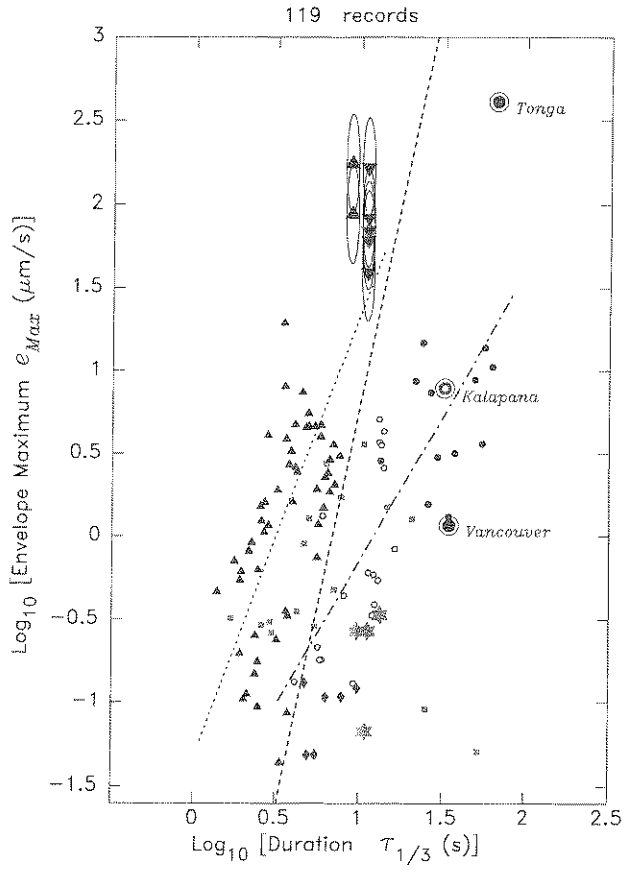

Figure 14

Same as Figure 6, but including the strong sources studied in Section 4. The data points previously used in the digital study are plotted in smaller size. In addition to the symbols used in Figure 6, the downward-pointing triangles are the presumed Vancouver explosions, the stars of David represent the 4 Christmas atmospheric nuclear tests and the circled symbols and labels identify the additional three earthquakes. Error ellipses are shown for the estimated parameters of the confirmed and presumed large-scale explosions. As on Figure 6, the dashed line is the separator (5). In addition, the dotted line represents the regression of the explosion data set (8.E), and the dash-dot line, that of the full earthquake data set (8.S-H); note that their slopes are different.

After regrouping the ten additional data points into the original data set, we computed the following linear regressions for the various types of records:

$$\log_{10} e_{\mathrm{Max}} = 2.67 \log_{10} \tau_{1/3} - 1.34 \qquad (8.\mathrm{E})$$

for the 60 explosion records (E and P);

$$\log_{10} e_{\mathrm{Max}} = 1.45 \log_{10} \tau_{1/3} - 1.44 \qquad (8.\mathrm{S})$$

for the 14 subduction earthquake records (S);

$$\log_{10} e_{\mathrm{Max}} = 2.01 \log_{10} \tau_{1/3} - 2.16 \qquad (8.\mathrm{H})$$

for the 19 hotspot earthquake records (H); and

$$\log_{10} e_{\mathrm{Max}} = 1.75 \log_{10} \tau_{1/3} - 1.90 \qquad (8.\mathrm{S\text{-}H})$$

when combining all 33 earthquake records (S and H).

Finally, we turn to the case of the four atmospheric nuclear tests at Christmas Island in June–July 1962. As shown on Figure 15, the paper records at PPT are unclipped and of sufficient quality to allow hand digitizing after optical magnification of the records. Classical data processing including removal of pen curvature yielded digital time series which were then processed through our standard algorithm. The spectrogram for the test of 10 July 1962 is shown at the bottom of Figure 15. As shown on Figure 14, where the four nuclear tests are plotted as stars of David, *T* waves from these atmospheric events differ substantially from those of underwater explosions, with all four data points falling on the "earthquake" side of the separator. Their characteristics are most similar to those of small intraplate earthquakes, and also to the later part of missile firing records, but they lack the high-frequency components found in the latter in the early parts of the records, and believed to originate in the underwater part of the firing sequence.

5. Conclusion and Perspective on the [e_{Max} : $\tau_{1/3}$] Discriminant

We have developed a discriminant based on the comparison of the maximum amplitude of ground velocity in a *T*-phase seismogram with the duration of the phase measured at 1/3 of its maximum. Measurements should be taken on the envelope of the seismogram along the procedure outlined above, and only stations on atolls, or at sites featuring a simple receiver-side conversion process, should be used. The discriminant, shown as the dashed line on Figure 14, successfully separates earthquakes from explosions. Other algorithms, notably those in the frequency domain, have a significant rate of failure, notably for intraplate earthquakes emanating from oceanic hotspot islands. The performance of the discriminant was tested successfully over 3.5 orders of magnitude of ground velocity by analyzing analog records of high-energy underwater explosions from the 1960s.

The proposed discriminant, e_{Max} *vs.* $\tau_{1/3}$ compares the maximum amplitude of the signal envelope, which is an instantaneous characteristic of its shape, with the duration at 1/3 of its maximum, which on the contrary, is related to the evolution with time of the signal, and hence, to a form of integral over time. Thus, the basic nature of the discriminant is rooted in the comparison of a higher-frequency parameter with a lower-frequency one, and its apparent success at separating

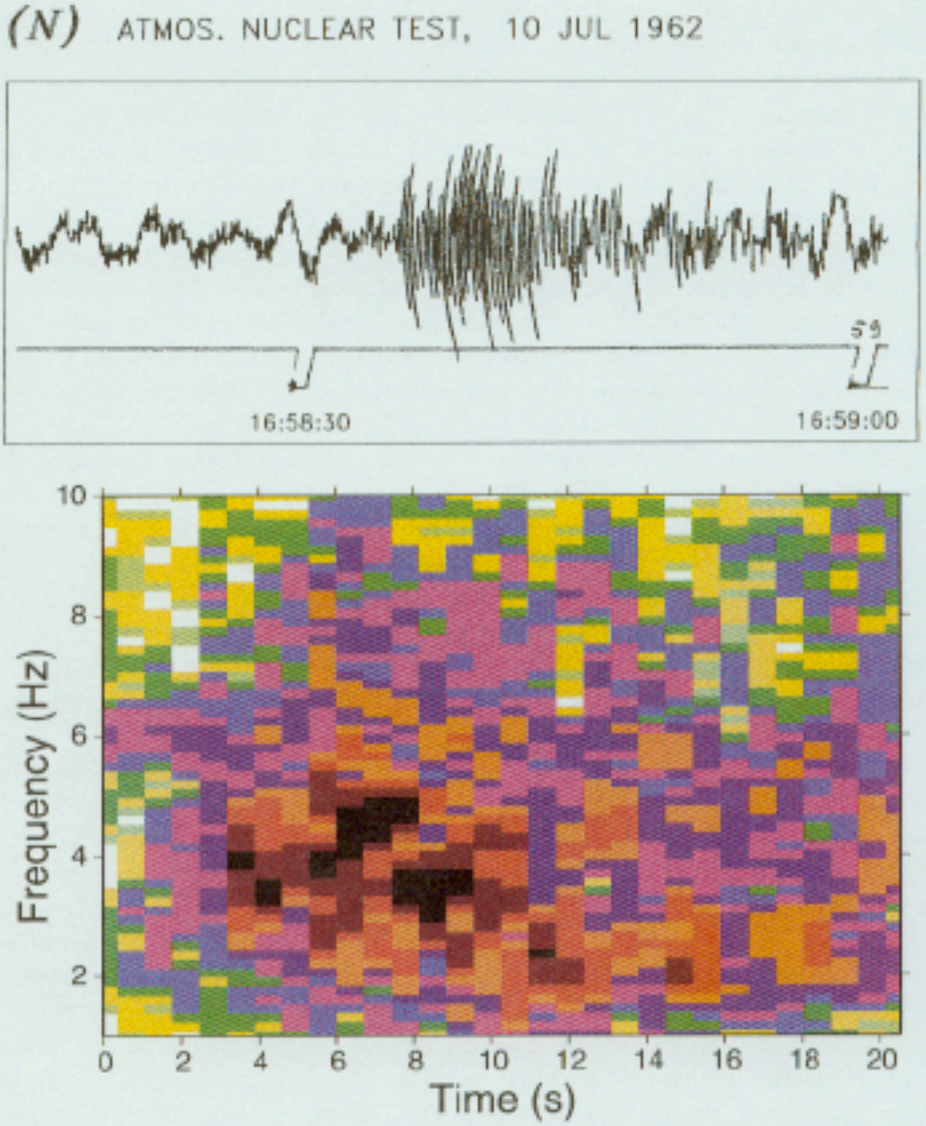

Figure 15

T wave recorded at Papeete from the atmospheric nuclear test at Christmas Island on 10 July 1962. *Top*: Original seismogram. The two tick marks are separated by 30 seconds. *Bottom*: Spectrogram obtained after hand-digitization of the record. Coding as on Figure 2.

earthquakes from explosions should not be surprising. (That it performs better than specific frequency-domain criteria remains intriguing.) Indeed, it shares a certain philosophy with such counterparts in land-based seismology as the time-honored m_b : M_s criterion (MARSHALL and BASHAM, 1972), or even the E/M_0 ratio between energy

and moment recently introduced by NEWMAN and OKAL (1998) to identify earthquakes with anomalously slow sources.

It would be desirable to cast the satisfactory performance of $[e_{Max} : \tau_{1/3}]$, observed over as much as 3.5 orders of magnitude of e, into the framework of a theoretical model of the generation of the T phases by both kinds of sources, and to provide some level of theoretical justification of Equations (8). However, this is a difficult endeavor since it requires the modeling of the growth with source size of four parameters, namely amplitude and time history of earthquakes and explosion sources. There exist models of either source and of the generation of the waves in the relevant medium. In the case of earthquakes, we face the formidable problem of the seismic-to-acoustic conversion, strongly affected by bathymetric features on a scale (a few hundred m) inaccessible to both mapping and modeling. Also, the two kinds of sources may not be directly comparable since an explosion will behave at least initially as a point source in the water, with an initially spherical growth of the wavefront (until trapped by the SOFAR channel), while an earthquake will illuminate a finite segment of conversion slope and thus behave initially as a line source for oceanic sound waves. Under these conditions, it is unclear that the two parameters generally computable from models of either source, namely the seismic ground motion at the source-side conversion shore (earthquake source) and the amplitude of the pressure pulse immediately outside the range of nonlinearity (explosion), can be simply related to the amplitudes of T phases eventually recorded at an on-shore seismic station.

Furthermore, the duration of the T phase is itself an *a priori* combination of the intrinsic duration of the source, the dispersion during propagation in the SOFAR channel, and the complexity of the conversion on the receiver side. The latter can be largely eliminated by considering only atoll stations. Dispersion will become prominent for signals with short source times and thus will more strongly affect explosion signals; furthermore, it could be feasible to effect a dispersion correction before taking the measurement of $\tau_{1/3}$; this improvement to the discriminant is presently being investigated.

In view of these difficulties, we give here only a very general perspective on the nature of the discriminant $[e_{Max} : \tau_{1/3}]$.

In the case of earthquakes, scaling models relating seismic displacements to earthquake size (e.g., GELLER, 1976) predict interference effects, followed by full saturation of the ground motion at any frequency f when the duration of the source becomes greater than $1/f$. Full saturation for a 5-Hz wave is expected at a seismic moment $M_0 = 10^{22}$ dyn-cm or $m_b = 4.4$ (rather than at the familiar 10^{28} dyn-cm for the Richter magnitude measured at a period 100 times longer). Destructive interference will start about one unit of magnitude below that, meaning that most earthquakes considered in this study will be affected. Hence, the amplitude of seismic motion and consequently of the T phase will grow slower than M_0. Similarly, while the duration of the source would be expected to grow as $M_0^{1/3}$, that of the T phase will

be primarily controlled by the duration of excitation of the scatterer at the solid-liquid interface. Consequently, the relationship between e_{Max} and $\tau_{1/3}$ is expected to mimic that existing between the amplitude of strong motion, a, and its duration, D, at a near-field receiver. Such (a, D) relations constitute the basis for the computation of so-called duration magnitudes (LEE *et al.*, 1972). While many variations of such scales have been proposed to adapt them to individual network studies, they generally use an algorithm of the form

$$M_D = b_0 + b_1 \log_{10} D \tag{9}$$

with b_1 varying from 1.5 in Southern California (REAL and TENG, 1973) to 2.8 in Puget Sound (CROSSON, 1972); for example, the preferred value $b_1 = 2.0$ (LEE and STEWART, 1981) would suggest a relationship of the form $\log_{10} a = 2 \log_{10} D$.

The slopes regressed from Equations (8), 2.01 for the mostly small H events, and 1.45 for the generally larger S ones, fall within the general range of used b_1 values, which confirms that the characteristics (amplitude and duration) of the T phases recorded from earthquakes are indeed rooted in those of the seismic ground motion at the seismic-to-acoustic conversion point.

In the case of explosions, we regressed the envelope amplitude e_{Max} as a function of the yield Y (in kg of TNT), as published for 44 sources, and obtained:

$$\log_{10} e_{Max} = 0.77 \log_{10} Y - 2.03 \tag{10}$$

the correlation coefficient being good (87%). The slope of the regression, 0.77, indicates that the amplitude of the recorded T phase grows significantly faster with yield than the amplitude p of the pressure pulse at the source: the latter has been modeled semi-empirically by COLE (1948) and CHAPMAN (1985) as growing like $(Y^{1/3})^{1.13} = Y^{0.38}$. This can be understood through the following argument: The pulse at the source is very narrow, decaying exponentially with a decay time θ_s which grows approximately like $Y^{1/3}(Y^{1/3})^{-0.22} = Y^{0.26}$ (CHAPMAN, 1985). By the time it is recorded with a dominant angular frequency ω at an island station, a T wave will have undergone what amounts to band-pass filtering, and the resulting recorded amplitude should be more directly related to the spectral amplitude $P(\omega)$ of the source pulse than to its time domain maximum, p. For an exponentially decaying signal, and in the limit $\omega\theta_s \ll 1$, we have $P(\omega) = p\theta_s$, which will then grow like $Y^{0.64}$. Of course, this model is very crude, since it assumes a constant ω, and ignores many factors such as the contribution of the secondary pulses (the so-called "bubble" effects), but it gives somes rationale to the observed fast growth of e_{Max} with Y.

As for the duration of the T phase, it is found to correlate poorly with yield (the coefficient being only 68%). This is probably due to the effects of dispersion on the shorter signals generated by explosions. Otherwise, one would expect the duration of the T wave to be controlled by the two characteristic times of the source, the decay time θ_s, and the period of the bubble, θ_B, the latter growing like $Y^{1/3}$. The ratio 0.77/(1/3) = 2.31 is not far removed from the value (2.67) regressed from the [$e_{Max} : \tau_{1/3}$] data set (Equation (8.E)).

It is evident that the arguments presented in this section fall short of a full satisfactory theoretical model of the performance of the proposed discriminant. Yet, they provide some level of justification for the observed slopes of regression on Figure 14. When event size is increased, the population of explosions, characterized by the steeper slope (2.67) is bound to separate from the earthquake group featuring an average slope of only 1.75. That this separation is effective in the range of event sizes considered here ($M > 3$ for earthquakes; $Y > 80$ kg for explosions) allows the discriminant to perform efficiently. Assuming that the same scaling laws apply, it is probable that the [$e_{Max} : \tau_{1/3}$] discriminant would fail for smaller events, in the yield range 1–10 kg and in the magnitude range 1–2.

Acknowledgments

This research is supported by the Defense Threat Reduction Agency of the Department of Defense, under Grant DSWA01-98-1-0007, and by Commissariat à l'Energie Atomique (France). The paper was improved through the comments of Jeffrey Stevens and another reviewer.

References

ANDO, M. (1979), *The Hawaii Earthquake of November 29, 1975: Low-dip Angle Faulting due to Forceful Injection of Magma*, J. Geophys. Res. *89*, 7616–7626.

ANONYMOUS (1989), *Announced United States Nuclear Tests, July 1945 through December 1988*, Office of External Affairs, U.S. Dept. of Energy, 64 pp.

CHAPMAN, N. R. (1985), *Measurement of Waveform Parameters of Shallow Explosive Charges*, J. Acoust. Soc. Am. *78*, 672–681.

COLE, R. H., *Underwater Explosions* (Princeton Univ. Press, Princeton, N.J., 1948), 437 pp.

CROSSON, R. S. (1992), *Small Earthquakes, Structure, and Tectonics of the Puget Sound Region*, Bull. Seismol. Soc. Am. *62*, 133–1171.

DUENNEBIER, F. K., and JOHNSON R. H. (1967), *T-phase Sources and Earthquake Epicenters in the Pacific Basin*, Hawaii Inst. Geophys. Rept. 67–24, 100 pp., Honolulu.

DZIEWONSKI, A. M., EKSTRÖM, G., and SALGANIK, M. P. (1996), *Centroid-moment Tensor Solutions for January–March 1995*, Phys. Earth Planet. Inter. *95*, 147–157.

DZIEWONSKI, A. M., EKSTRÖM, G., and SALGANIK, M. P. (1997a), *Centroid-moment Tensor Solutions for October–December 1995*, Phys. Earth Planet. Inter. *101*, 1–12.

DZIEWONSKI, A. M., EKSTRÖM, G., and SALGANIK, M. P. (1997b), *Centroid-moment Tensor solutions for January–March 1996*, Phys. Earth Planet. Inter. *102*, 1–9.

DZIEWONSKI, A. M., EKSTRÖM, G., and SALGANIK, M. P. (1997c), *Centroid-moment Tensor Solutions for April–June 1996*, Phys. Earth Planet. Inter. *102*, 11–20.

DZIEWONSKI, A. M., EKSTRÖM, G., MATERNOVSKAYA, N. N., and SALGANIK, M. P. (1997d), *Centroid-moment Tensor Solutions for July–September 1996*, Phys. Earth Planet. Inter. *102*, 133–143.

DZIEWONSKI, A. M., EKSTRÖM, G., and MATERNOVSKAYA, N. (1998), *Centroid-moment Tensor Solutions for October–December 1996*, Phys. Earth Planet. Inter. *105*, 95–108.

DZIEWONSKI, A. M., EKSTRÖM, G., and MATERNOVSKAYA, N. (1999a), *Centroid-moment Tensor Solutions for April–June 1997*, Phys. Earth Planet. Inter. *112*, 1–9.

DZIEWONSKI, A. M., EKSTRÖM, G., and MATERNOVSKAYA, N. (1999b), *Centroid-moment Tensor Solutions for July–September 1997*, Phys. Earth Planet. Inter., in press.

GELLER, R. J. (1976), *Scaling Relations for Earthquake Source Parameters and Magnitudes*, Bull. Seismol. Soc. Amer. *66*, 1501–1523.

LEE, W. H. K., and STEWART, S. W., *Principles and Applications of Microearthquake Networks*, Adv. Geophys. Suppl. 2, 293 pp. (Academic Press, New York, 1981).

LEE, W. H. K., BENNETT, R. E., and MEAGHER, K. L. (1972), *A Method of Estimating Magnitude of Local Earthquakes from Signal Duration*, U.S. Geol. Surv. Open File Rept., 28 pp.

LINEHAN, J. (1946), *Earthquakes in the West Indian Region*, Trans. Am. Geophys. Un. *21*, 229–232.

LUNDGREN, P. R., and OKAL, E. A. (1988), *Slab Decoupling in the Tonga Arc: The June 22, 1977 Earthquake*, J. Geophys. Res. *93*, 13,355–13,366.

MA, K.-F., KANAMORI, H., and SATAKE, K. (1999), *Mechanism of the 1975 Kalapana, Hawaii Earthquake Inferred from Tsunami Data*, J. Geophys. Res. *104*, 13,153–13,167.

MARSHALL, P. D., and BASHAM, P. W. (1972), *Discrimination between Earthquakes and Underground Explosions Using an Improved M_s Scale*, Geophys. J. Roy. astr. Soc. *28*, 431–458.

NAVA, F. A., NÚÑEZ-CORNÚ, F., CÓRDOBA, D., MENA, M., ANSORGE, J., RODRÍGUEZ, M., BANDA, E., MÜLLER, S., UDÍAS, A., GARCI'A-GARCÁ, M., CALDERÓN, G., and the MEXICAN WORKING GROUP FOR DEEP SEISMIC PROFILING, (1988), *Structure of the Middle America Trench in Oaxaca, Mexico*, Tectonophy. *154*, 241–251.

NEWMAN, A. V., and OKAL, E. A. (1998), *Teleseismic Estimates of Radiated Seismic Energy: The E/M_0 Discriminant for Tsunami Earthquakes*, J. Geophys. Res. *103*, 26,885–26,898.

OKAL, E. A. (1989), *A Theoretical Discussion of Time-domain Magnitudes: The Prague Formula for M_s and the Mantle Magnitude M_m*, J. Geophys. Res. *94*, 4194–4204.

OKAL, E. A., and TALANDIER, J. (1986), *T-wave Duration, Magnitudes and Seismic Moment of an Earthquake; Application to Tsunami Warning*, J. Phys. Earth *34*, 19–42.

PISERCHIA, P.-F., VIRIEUX, J., RODRIGUES, D., GAFFET, S., and TALANDIER, J. (1998), *Hybrid Numerical Modeling of T-wave Propagation: Application to the Midplate Experiment*, Geophys. J. Intl. *133*, 789–800.

RAVET, J. (1940), *Remarques sur quelques enregistrements d'ondes à très courte période au cours de tremblements de terre lointains à l'Observatoire du Faiere, Papeete, Tahiti*, Sixth Pacific Sci. Congress, vol. 1, pp. 127–130.

REAL, C. R., and TENG, T.-L. (1973), *Local Richter Magnitude and Total Signal Duration in Southern California*, Bull. Seismol. Soc. Am. *63*, 1809–1827.

TALANDIER, J. (1993), *French Polynesia Tsunami Warning Center (CPPT)*, Natural Hazards *7*, 237–256.

TALANDIER, J., and OKAL, E. A. (1982), *Crises sismiques au volcan Macdonald (Océan Pacifique Sud)*, C.R. Acad. Sci. Paris, Sér. II. *295*, 195–200.

TALANDIER, J., and OKAL, E. A. (1984a), *The Volcanoseismic Swarms of 1981–1983 in the Tahiti-Mehetia Area, French Polynesia*, J. Geophys. Res. *89*, 11,1216–11,234.

TALANDIER, J., and OKAL, E. A. (1984b), *New Surveys of Macdonald Seamount, Southcentral Pacific, Following Volcanoseismic Activity, 1977–1983*, Geophys. Res. Lett. *11*, 813–816.

TALANDIER, J., and OKAL, E. A. (1987a), *Seismic Detection of Underwater Volcanism: The Example of French Polynesia*, Pure appl. geophys. *125*, 919–950.

TALANDIER, J., and OKAL, E. A. (1987b), *Crustal Structure in the Tuamotu and Society Islands, French Polynesia*, Geophys. J. Roy. astr. Soc. *88*, 499–528.

TALANDIER, J., and OKAL, E. A. (1998), *On the Mechanism of Conversion of Seismic Waves to and from T Waves in the Vicinity of Island Shores*, Bull. Seismol. Soc. Am. *88*, 621–632.

WEIGEL, W., *Bericht über die SONNE-Expedition SO65-2, Papeete-Papeete, 7.-28. Dez. 1989* (Universität Hamburg, Institut für Geophysik, 1990).

(Received June 30, 1999, revised November 8, 1999, accepted November 15, 1999)

To access this journal online:
http://www.birkhauser.ch